



Deposited via The University of Sheffield.

White Rose Research Online URL for this paper:

<https://eprints.whiterose.ac.uk/id/eprint/186375/>

Version: Accepted Version

Article:

Hasanali, M., Mojtabaei, S.M., Clifton, G.C. et al. (2022) Capacity and design of cold-formed steel warping-restrained beam-column elements. *Journal of Constructional Steel Research*, 190. 107139. ISSN: 0143-974X

<https://doi.org/10.1016/j.jcsr.2022.107139>

Article available under the terms of the CC-BY-NC-ND licence
(<https://creativecommons.org/licenses/by-nc-nd/4.0/>).

Reuse

This article is distributed under the terms of the Creative Commons Attribution-NonCommercial-NoDerivs (CC BY-NC-ND) licence. This licence only allows you to download this work and share it with others as long as you credit the authors, but you can't change the article in any way or use it commercially. More information and the full terms of the licence here: <https://creativecommons.org/licenses/>

Takedown

If you consider content in White Rose Research Online to be in breach of UK law, please notify us by emailing eprints@whiterose.ac.uk including the URL of the record and the reason for the withdrawal request.

Capacity and design of cold-formed steel warping-restrained beam-column elements

Maryam Hasanali^{a*}, Seyed Mohammad Mojtabaei^b, G.Charles Clifton^a, Iman Hajirasouliha^b,
Shahabeddin Torabian^c, James B.P. Lim^a

^a Department of Civil and Environmental Engineering, The University of Auckland, New Zealand

^b Department of Civil and Structural Engineering, The University of Sheffield, Sheffield, UK

^c Department of Civil Engineering, Johns Hopkins University, Baltimore, MD, USA

* Corresponding author: mhas455@aucklanduni.ac.nz

Abstract

In current design standards, cold-formed steel (CFS) beam-column elements are generally designed by considering fully warping free behaviour in their supports, which means the benefit of warping-restrained boundary conditions is neglected. In addition, while a non-linear relationship governs the interaction of axial compression and bending, simplified linear expressions are prescribed in design standards, which may lead to unreliable designs. This paper aims to investigate the efficiency of the well-known Direct Strength Method (DSM) as well as the methods proposed by previous researchers for CFS warping-restrained beam-column members. The results of experimentally validated warping-restraint Finite Element (FE) models, considering material nonlinearity and geometric imperfections, are used as a benchmark. A total of 270 CFS elements with various lengths, thicknesses and cross-sectional dimensions are considered under ten different load eccentricity levels. The results are then employed to investigate the effects of warping-restrained boundary conditions as well as code recommended interaction curves on the efficiency of the existing methods to estimate the strength of CFS beam-columns with warping restraint. The results indicate that the estimated capacity of CFS beam-columns is significantly affected (up to 55%) by the warping restraint effects and the errors associated with using the simple linear interaction curve, depending on

26 the element length and thickness. While the influence of warping restraint is generally less than
27 6%, it is demonstrated that, on average, all existing design methods underestimate the capacity
28 of CFS beam-columns by at least 20%, which highlights the need to develop more accurate
29 design methods for practical design purposes.

30

31 **Keywords:** Cold-formed steel, Beam-columns, Warping-restrained boundary conditions,
32 Direct Strength Method (DSM), Finite element (FE) model

33 **1 Introduction**

34 Cold-formed steel (CFS) members have been traditionally employed as secondary
35 elements, such as roof purlins, wall girts and cladding or as wall studs in non-structural internal
36 walls in multi-storey buildings. However, CFS members are increasingly being used in the
37 structural systems of low to mid-rise buildings, including shear-wall panels and moment-
38 resisting portal frames [1, 2] due to their structural and environmental advantages, such as their
39 high strength-to-weight ratio, flexibility in cross-sectional shapes, ease of assembly,
40 transportation and recyclability [3].

41 In most structural system applications, CFS structural members are subjected to
42 combined axial compression and bending (see Fig. 1(a)) both in moment resisting frames [4,
43 5] and stud wall systems [6, 7]. CFS compression members are also highly susceptible to
44 eccentric loads due to their thin-walled open cross-sections, an example as shown in Fig. 1(b).
45 This can generate combined axial compression and bending moments and consequently alter
46 the behaviour and failure mechanism of CFS members [8-10].

47 The behaviour of CFS beam-column members under various load combinations has been
48 experimentally and numerically investigated in the literature. Torabian et al. [9, 10] conducted

49 55 experimental tests on warping restrained lipped channel-sections and 43 tests on Z-sections
50 under axial compression and bi-axial moments; using the results of these tests the reliability of
51 the American Iron and Steel Institute (AISI S100 (2012)) [11] was assessed. They showed that
52 the use of linear interaction expressions for the beam-columns is excessively conservative. In
53 another study, Cheng et al. [12] analytically investigated lateral-torsional buckling of CFS
54 lipped channel sections subjected to combined axial compression and bending about their
55 major and minor axes. It was demonstrated that the bending moment decreases the critical
56 compression load for a section subject to combined compression and the major-axis bending,
57 while the effect of minor-axis bending moment on the critical compression load depends on
58 the direction of applied bending. The critical value of the compression load will be reduced
59 when the direction of minor axis bending moment puts the lips into compression, whereas the
60 direction of bending moment creating the compression in the web has almost no effect on the
61 critical value of the compression load, unless the magnitude of the applied moment is very
62 close to the design member moment capacity. A comprehensive experimental program was
63 conducted by Ma et al. [13] on 51 high-strength CFS beam-column elements with square and
64 rectangular hollow sections and the results were used to compare the accuracy of the
65 predictions obtained from American [14], European [15], and Australian design provisions
66 [16]. More recently, Li and Young [17] experimentally investigated the behaviour of 33 CFS
67 built-up open section beam-columns under different eccentric loads. They reported that the
68 AISI S100 (2016) [21], AS/NZS 4600 (2018) [22], EN 1993-1-1 (2005) [15] and ANSI/AISC
69 360 (2010) [14] generally underestimate the strengths of the CFS built-up beam-column
70 members. With regards to the optimisation of CFS beam-column elements, a number of
71 research studies were also devoted to identify optimum cross-sectional shapes and dimensions
72 of single and built-up beam-columns to maximise their load-bearing capacity under various
73 load combinations [18-20].

74 The majority of these experimental studies focused on CFS beam-column members with
75 restrained warping at their supports, which is consistent with the way these elements are
76 generally used in the construction practice (e.g., studs in shear wall panels). However, the AISI
77 S100 (2016) [21] and AS/NZS 4600 (2018) [22] only prescribe simple linear interaction
78 equations for beam-column elements. To address this issue, Moen [23] and Rajkannu and
79 Jayachandran [24] proposed different methods to take into account the effects of warping
80 restraint in CFS compressive members. However, these methods were developed based on
81 limited number of cases; and therefore, there is a need to assess their efficiency for a wider
82 range of elements and load conditions.

83 This paper aims to provide a better understanding about the effects of warping-restrained
84 boundary conditions on the behaviour and failure mechanism of CFS beam-column elements
85 and evaluate the reliability of the Direct Strength Method (DSM) as specified in AISI S100
86 (2016) [21] and AS/NZS 4600 (2018) [22] as well as design proposals found in the literature.
87 To this end, detailed nonlinear Finite Element (FE) models of CFS beam-column members
88 under different load combinations are developed by taking into account material nonlinearity
89 and geometric imperfections and validated based on the results of existing experimental tests.
90 The validated models are then used for the parametric studies on the key design parameters of
91 beam-column members, including length (i.e., 0.5, 1.5, 3 m), thickness (i.e., 1, 2, 4 mm) and
92 cross-sectional dimensions subjected to ten different load eccentricities (in total 270
93 specimens). The results are then employed to investigate the effects of warping-restrained
94 boundary conditions on the strength of CFS beam-columns and subsequently assess the
95 interactions curves and accuracy of the existing methods for estimation of their capacity.

96 **2 Current design methods for CFS members**

97 The two main methodologies which are generally available in the current design
98 guidelines for CFS members are the Effective Width Method (EWM) (AISI 1996) [25] and the
99 Direct Strength Method (DSM) (AISI 2004) [26]. While the DSM is mainly adopted in AISI
100 S100 (2016) [21] and AS/NZS 4600 (2018) [22], the EWM is prescribed in the majority of
101 CFS design standards including EN 1993-1-3 (2006) [27], AISI S100 (2016) [21] and AS/NZS
102 4600 (2018) [22]. The EWM uses reduced cross-section properties along with the yield stress;
103 however, the DSM employs the gross cross-section properties in conjunction with a direct
104 reduced strength based on the stability of the gross cross-section [28]. The comparison between
105 the strength predictions of EWM and DSM against the experimental results of lipped channel
106 columns revealed that the test-to-predicted ratio can vary from 0.6 to 1.3 [28, 29]. In a recent
107 study, a framework was developed to predict the axial capacity of CFS channel sections using
108 Deep Belief Network (DBN) [30]. Comparison of the results with the EWM and DSM
109 estimations confirmed that these methods are generally conservative by around 15%.

110 *2.1 DSM*

111 The Direct Strength Method was first presented by Schafer and Peköz [29] as an
112 alternative to the traditional effective width method to predict the load-carrying capacities of
113 CFS members. In this method, the capacity of a CFS member is determined by utilizing the
114 yield strength of the member and the elastic stability of the cross-section (i.e., local,
115 distortional, and global buckling) using empirical relationships. To predict elastic critical
116 buckling strength, finite strip analysis is performed by using CUFSM [32] or Thin-Wall [33]
117 software. In this section, the prediction of buckling resistance for different warping-free CFS
118 structural elements (i.e., column, beam and beam-column) are briefly described.

119 2.1.1 Buckling resistance of column elements

120 According to AISI S100 (2016) [21], axial compressive resistance for global buckling is
 121 expressed in terms of compressive yield load, $P_y = A_g f_y$, and slenderness ratio $\lambda_c = \sqrt{P_y/P_{cre}}$
 122 (where A_g is the gross cross-sectional properties, f_y is the yield stress, and P_{cre} denotes the
 123 elastic global buckling strength):

$$\begin{cases} P_{ne} = (0.658^{\lambda_c^2}) P_y & \text{for } \lambda_c \leq 1.5 \\ P_{ne} = \left(\frac{0.877}{\lambda_c^2}\right) P_y & \text{for } \lambda_c > 1.5 \end{cases} \quad (1)$$

124 where P_{ne} is the nominal member compression capacity for flexural, torsional, and flexural-
 125 torsional buckling.

126 AISI S100 (2016) [21] takes into account the local-global interaction mode through the
 127 local-global slenderness ratio $\lambda_l = \sqrt{P_{ne}/P_{crl}}$, and therefore, the nominal axial resistance for
 128 local buckling is defined by [21]:

$$\begin{cases} P_{nl} = P_{ne} & \text{for } \lambda_l \leq 0.776 \\ P_{nl} = \left[1 - 0.15 \left(\frac{P_{crl}}{P_{ne}}\right)^{0.4}\right] \left(\frac{P_{crl}}{P_{ne}}\right)^{0.4} P_{ne} & \text{for } \lambda_l > 0.776 \end{cases} \quad (2)$$

129 The nominal axial resistance for distortional buckling is expressed in terms of distortional
 130 buckling slenderness ratio $\lambda_d = \sqrt{P_y/P_{crd}}$:

$$\begin{cases} P_{nd} = P_y & \text{for } \lambda_d \leq 0.561 \\ P_{nd} = \left[1 - 0.25 \left(\frac{P_{crd}}{P_y}\right)^{0.6}\right] \left(\frac{P_{crd}}{P_y}\right)^{0.6} P_y & \text{for } \lambda_d > 0.561 \end{cases} \quad (3)$$

131 The nominal axial resistance of the compression member (P_n) is then predicted by using
 132 the minimum value of the resistances determined in Eqs. (1) to (3).

133 *2.1.2 Buckling resistance of beam elements*

134 Based on AISI S100 (2016) [21] regulations, the nominal flexural resistance is
 135 determined through the flexural yield moment $M_y = W_y f_y$ and the elastic critical lateral-
 136 torsional moment M_{cre} (where W_y is the elastic section modulus, termed Z_y in AS/NZS 4600
 137 [22]):

$$\begin{cases} M_{ne} = M_{cre} & \text{for } M_{cre} < 0.56M_y \\ M_{ne} = \frac{10}{9}M_y \left(1 - \frac{10M_y}{36M_{cre}}\right) & \text{for } 2.78M_y \geq M_{cre} \geq 0.56M_y \\ M_{ne} = M_y & \text{for } M_{cre} > 2.78M_y \end{cases} \quad (4)$$

138 The nominal flexural resistance for local buckling considering local-global interaction is
 139 also expressed as a function of the local-global slenderness ratio $\lambda_l = \sqrt{M_{ne}/M_{crl}}$:

$$\begin{cases} M_{nl} = M_{ne} & \text{for } \lambda_l \leq 0.776 \\ M_{nl} = \left[1 - 0.15 \left(\frac{M_{crl}}{M_{ne}}\right)^{0.4}\right] \left(\frac{M_{crl}}{M_{ne}}\right)^{0.4} M_{ne} & \text{for } \lambda_l > 0.776 \end{cases} \quad (5)$$

140 The nominal flexural resistance for distortional buckling is determined using distortional
 141 buckling slenderness ratio $\lambda_d = \sqrt{M_y/M_{crd}}$:

$$\begin{cases} M_{nd} = M_y & \text{for } \lambda_d \leq 0.673 \\ M_{nd} = \left[1 - 0.22 \left(\frac{M_{crd}}{M_y}\right)^{0.5}\right] \left(\frac{M_{crd}}{M_y}\right)^{0.5} M_y & \text{for } \lambda_d > 0.673 \end{cases} \quad (6)$$

142 The nominal flexural resistance of the CFS member (M_n) is then obtained from the
 143 minimum value of the resistances determined in Eqs. (4) to (6).

144 *2.1.3 Buckling resistance of beam-column elements*

145 AISI S100 (2016) [21] recommends two linear interaction equations for the warping-free
 146 CFS members under combined axial compression and bending moments:

$$\frac{P}{P_n} + \frac{M_x}{M_{nx}} + \frac{M_y}{M_{ny}} \leq 1.0 \quad (7)$$

147 In the above equation P , M_x and M_y are defined as the applied axial compression load
148 and bending moments about the x and y-axes, respectively. P_n is denoted as available axial
149 compressive capacity, while M_{nx} and M_{ny} are available flexural strength about the x and y-
150 axes, respectively.

151 *2.2 DSM with warping-restrained elastic Buckling resistances*

152 To take into account the effects of warping restrained boundary conditions, the elastic
153 critical buckling loads and bending moments of the DSM equations can be replaced with those
154 obtained for warping restrained boundary conditions [19]. Based on this method, the warping
155 restrained CFS element can be modelled in Finite Element (FE) software (e.g., ABAQUS [34])
156 under pure axial load and pure bending moments in major and minor axes. The eigenvalues
157 obtained from the FE analyses are then employed to predict the capacities through the DSM
158 equations.

159 *2.3 Proposed design method by Moen*

160 Moen [23] investigated the effects of warping deformation on the column cross-sections
161 through experimental and analytical studies and reported that the warping-fixed boundary
162 conditions can lead to shortening the distortional buckling half-wavelength. This results in an
163 amplification of the elastic critical distortional buckling load (P_{crd}) of the column members. It
164 was also demonstrated that the magnitude of the boost in P_{crd} decreases by increasing the
165 column length, since the wavelength shortening required to accommodate distortional buckling
166 in the column can be distributed over multiple half-waves in which the flange can rotate in plan
167 going from one half wavelength into the adjacent half wavelength.

168 Based on the results of their study, Moen [23] updated DSM equations for warping
 169 restrained CFS columns by proposing a boosting factor that enhances the elastic critical
 170 distortional buckling load (P_{crd}), while the critical elastic local buckling load (P_{crl}) remains
 171 unchanged. The boosting factor, which is applied on the distortional critical buckling load
 172 (P_{crd}), is given by Eq. (8), where L_{crd} is the distortional half-wavelength and L is unbraced
 173 length of the member.

$$D_{boost} = 1 + \frac{1}{2} \left(\frac{L_{crd}}{L} \right)^2 \quad (8)$$

174 2.4 Proposed design method by Rajkannu & Jayachandran

175 In a more recent study, Rajkannu and Jayachandran [24] studied the effects of warping
 176 on the flexural-torsional buckling behaviour of the CFS lipped-channel sections under pure
 177 axial compression experimentally and numerically. It was concluded that the compressive
 178 strength and failure modes may significantly change by restraining warping, and consequently,
 179 the current DSM predictions for flexural-torsional buckling strength can be very conservative.
 180 In this study, warping restraint factors w_i and w_e for inelastic and elastic region, respectively,
 181 were proposed as given in Eq. (9) to modify the strength predicted by DSM for global buckling
 182 of the axial compressive element (P_{ne}).

$$P_{ne} = \begin{cases} (w_i \times 0.658^{\lambda_c^2}) P_y & \text{for } \lambda_c \leq 1.5 \\ \left(\frac{w_e \times 0.877}{\lambda_c^2} \right) P_y & \text{for } \lambda_c > 1.5 \end{cases} \quad (9)$$

183 In the above equation, $w_i = w_e = 1$ for the members failing in flexure buckling, and w_i
 184 $= 1.27$, $w_e = 1.9$ for the members failing in flexural-torsional buckling.

185 To predict the dominant buckling mode, a threshold was proposed using the ratio x_o/b ,
 186 where x_o is the distance between the centroid and shear centre of the cross-section and b is the
 187 cross-sectional flange width. If $x_o/b > 0.75 + 0.7(d/b)$, the member fails in flexural-

188 torsional buckling (d is the dimension of cross-sectional lips), while the member fails in
 189 flexural buckling if $x_o/b < 0.75 + 0.7(d/b)$. It was demonstrated that the strength of
 190 members failing in flexural buckling is independent of the warping restraint conditions. It
 191 should be mentioned that this method failed to consider the effects of the warping-fixed
 192 boundary condition on the capacity of the members studied herein as none of the failure modes
 193 of these cross-sections was flexural-torsional buckling in compression loading conditions.

194 *2.5 Proposed design method by Torabian and Schafer*

195 While the design of CFS beam-column members is on the basis of a linear interaction of
 196 axial compression and bending moments, Torabian & Schafer [8] and Torabian et al. [9]
 197 extended the DSM in order to take into account the actual stresses generated by combined
 198 actions. In fact, the actual stress distributions resulted from both compression and bending are
 199 used in a buckling analysis to determine the critical buckling parameters [8]. In this method,
 200 the applied axial compression and bending moments are first normalised to the cross-sectional
 201 yield strength (M_{1y}, M_{2y}, P_y), and then the normalized points are shifted from x, y and z
 202 coordinates to an azimuth angle (θ_{MM}), an elevation angle (ϕ_{PM}) and a radial length (β),
 203 respectively:

$$\theta_{MM} = \tan^{-1}(y/x), \phi_{PM} = \cos^{-1}(z/\beta), \beta = \sqrt{x^2 + y^2 + z^2} \quad (10)$$

204 For any required action ($P_r - M_{1r} - M_{2r}$), the following parameters are defined:

$$x_r = \frac{M_{1r}}{M_{1y}}, y_r = \frac{M_{2r}}{M_{2y}}, z_r = \frac{P_r}{P_y} \quad (11)$$

$$\theta_{MM} = \tan^{-1}(y_r/x_r), \phi_{PM} = \cos^{-1}(z_r/\beta_r), \beta_r = \sqrt{x_r^2 + y_r^2 + z_r^2} \quad (12)$$

205 Therefore, the state of the stress on the cross-section can be determined as follows:

$$\sigma_r = \frac{P_r}{A} + \frac{M_{1r}y_{c2}}{I_1} + \frac{M_{2r}y_{c1}}{I_2} \quad (13)$$

206 where σ_r is the required axial stress under combined required actions (P_r , M_{1r} and M_{2r}), y_{c1}
 207 and y_{c2} are the distance to the centroidal principal axes 1 and 2, respectively, and A , I_1 , and I_2
 208 are the cross-sectional area, and the moment of inertia about axes 1 and 2, respectively.

209 By obtaining the maximum required axial stress σ_{r-max} from Eq. (13), the yielding actions
 210 ($\beta_y, \theta_{MM}, \phi_{PM}$) can be determined as follows:

$$|\sigma_r(y_{c1}, y_{c2})|_{max} \times \alpha_y = F_y \quad (14)$$

$$\alpha_y = \frac{F_y}{\sigma_{r-max}} \quad (15)$$

$$\beta_y = \alpha_y \beta_r \quad (16)$$

211 where F_y is the yield stress, β_y represent the first yield of the members. Cross-section stability
 212 analysis performed on σ_r provides elastic buckling load factors for local (α_{crL}), distortional (α_{crD})
 213 and global (α_{crG}) buckling. Using the elastic buckling load factor, elastic buckling
 214 strength under the combined actions ($\beta_r, \theta_{MM}, \phi_{PM}$) are as follows:

$$\beta_{crL} = \alpha_{crL} \beta_r \quad (17)$$

$$\beta_{crD} = \alpha_{crD} \beta_r \quad (18)$$

$$\beta_{crG} = \alpha_{crG} \beta_r \quad (19)$$

215 where β_{crG} , β_{crD} and β_{crL} show the elastic buckling values for global, distortional and local
 216 elastic buckling, respectively. Nominal strength (β_n) is, therefore, the minimum of the member
 217 strength in local, distortional and global buckling.

218 **3 Description of Finite Element (FE) models**

219 FE analysis has been frequently proved to be an efficient tool in predicting the behaviour
 220 and strength of CFS elements and structural components [35-37]. In this study, detailed

221 nonlinear FE models of CFS elements under various loading conditions have been developed
222 using ABAQUS software [34] by considering the material nonlinearity and geometric
223 imperfections. The models have then been validated based on the results of two experimental
224 programs: (i) CFS elements under pure axial compression (i.e. columns) tested by Ye et al. [38]
225 at the University of Sheffield and (ii) CFS elements under combined axial compression and
226 bending moments (i.e., beam-columns) conducted by Torabian et al. [39] at Johns Hopkins
227 University. It should be mentioned that while Torabian et al. [39] also conducted pure axial
228 compression tests, they did not obtain good agreements between the results of their experiments
229 and the corresponding FE models, due to some uncertainties such as the existence of the global
230 twist imperfection. Therefore, it was decided to use two different experimental tests to validate
231 the FE models adopted in this study.

232 *3.1 Specimens, boundary conditions and loading*

233 Ye et al. [38] tested pinned-ended warping-restrained CFS columns with different lengths
234 and cross-sectional dimensions under concentric axial compressive loads. To simulate the
235 adopted test setup, a 38 mm thick solid plate with an arc-shaped groove and a cylinder roller
236 with a radius of 12 mm embedded inside the groove were modelled at both ends of the
237 specimens as the hinge assemblies, as shown in Fig. 2. The contacts were defined between: (i)
238 the column specimen and the endplate and (ii) the roller and end plate (see Fig. 2). A node-to-
239 surface contact pair was used to define the interaction between the column specimen and the
240 endplate, where combined “hard” and “rough” contact behaviour were assigned in normal and
241 tangential directions to avoid any penetration and tangential slip between the surfaces,
242 respectively [34]. A surface-to-surface contact property was also used to define the interaction
243 of the endplate and roller. While “hard” contact was defined in the normal direction, the contact
244 in the tangential direction was set to “penalty” to take into account the effects of friction
245 between the roller and endplate. Based on the sensitivity analyses conducted in [31], the most

246 appropriate friction factor to achieve convergence was obtained to be equal to 0.2. The
247 sensitivity analysis demonstrated that the predicted compressive capacity decreases with the
248 reduction of friction factor, whereas no significant drop of the peak load was observed using
249 friction factors smaller than 0.2. Moreover, a friction factor of 0.2 provided an excellent
250 agreement between the experimental and numerical results. At each end of the member, the
251 nodes of the top surface of the roller which is in contact with the groove were coupled to the
252 reference point with fixed boundary conditions.

253 Torabian et al. [39] tested a set of CFS beam-column members under eccentric axial
254 compressive loads in order to generate combined actions (i.e., compression and bending
255 moments) on the elements. One reference point was placed at each end of the member and the
256 coordinate of the reference point was varied as different eccentricities applied to the specimen.
257 A rigid link with a length of 152.4 mm was created between the reference point and the
258 specimen end to simulate the depth of the clevis used in the test set-up. All degrees of freedom
259 of each end cross-section were then coupled to its corresponding reference point pinned about
260 the minor and major axis, as shown in Fig. 3.

261 *3.2 Element type and material properties*

262 A nine-node shell element with reduced integration, *S9R5*, selected from the ABAQUS
263 element library [34] was assigned to both column and beam-column members. Each node of
264 this element type has three translational degrees of freedom and two in-surface rotational
265 degrees of freedom. Based on the investigations conducted by Schafer et al. [41], this element
266 type can provide accurate predictions for thin-walled structures. An 8-node linear brick element
267 with reduced integration (*C3D8R*) and hourglass control was also used for the modelling of the
268 endplates and rollers. Following a comprehensive mesh sensitivity analysis, the element sizes
269 of $10 \times 10 \text{ mm}^2$ were found to be suitable for the flat regions of the CFS columns under pure

270 compression and beam-column elements subjected to combined compression and bending
271 moments, while four elements were used in the radial direction of the corners. To show the
272 results of mesh sensitivity analysis, the load-displacement responses of one of the CFS
273 members (i.e., B1500-c cross-section adapted from Ye et al. [38]) with various mesh sizes are
274 demonstrated in Fig. 4.

275 In general, the ultimate capacity and post-buckling behaviour of CFS elements can be
276 significantly affected by the inelastic properties of CFS material [40]. In this study, the
277 behaviour of CFS elements was simulated by using a bi-linear stress-strain model. To model
278 the CFS column elements, the elastic Young's modulus of $E = 196$ GPa and the yield stress of
279 $F_y = 440$ MPa were used based on the results of coupon tests [38]. Similarly, the measured
280 elastic Young's modulus of $E = 203.4$ GPa and the yield stress of $F_y = 365$ MPa were also
281 used for beam-column members [39]. The Poisson ratio was taken equal to 0.3 for both column
282 and beam-column members. It should be noted that the obtained engineering stress-strain
283 curves were converted to true stress and true strain data using the following equation:

$$\begin{cases} \varepsilon_{true} = \ln(1 + \varepsilon_e) \\ \sigma_{true} = \sigma_e(1 + \varepsilon_e) \end{cases} \quad (20)$$

284 where σ_e and ε_e are the measured engineering stress and strain data based on the original cross-
285 sectional area of the coupons. Fig. 5 compares the engineering and the true stress-strain curves
286 of the tested column and beam-column elements.

287 With respect to the roll-forming/cold-work effect, generally cold-formed structural
288 sections are manufactured by rolling process, causing residual stress and increasing the material
289 yield stress in the corner zones. It has previously been demonstrated that the effects of
290 membrane residual stresses can safely be neglected in open sections [40, 41] while the
291 (longitudinal) bending residual stresses are implicitly accounted for in the coupon test results,

292 provided that the coupons are cut from the fabricated cross-section rather than from the virgin
293 plate. Indeed, cutting a coupon releases the bending residual stresses, causing the coupon to
294 curl [41]. However, these stresses are re-introduced when the coupon is straightened under
295 tensile loading in the initial stages of the coupon test.

296 *3.3 Geometric imperfections*

297 It has been previously shown that the initial geometric imperfections can have
298 considerable effects on the strength and post-buckling behaviour of CFS elements [42, 43]. The
299 general shape of imperfections can be generally determined according to the dominant buckling
300 mode shape (i.e., local, distortional, and global) obtained from elastic buckling analysis [29].
301 In this study, the Finite Strip Method was first performed through CUFSM software [32] to
302 predict the dominant buckling mode shape and its corresponding half-wavelength for each
303 element. Following the above procedure, a program was developed in Matlab [44] for the
304 inclusion of imperfections and generating of nodal coordinates in ABAQUS [34]. The
305 magnitude of the cross-sectional deformed shape was then scaled to certain values depending
306 on the thickness of the elements. Based on the work conducted by Schafer and Peköz [40] for
307 cross-sections with a thickness (t) smaller than 3 mm, the amplitudes of imperfections for local
308 and distortional buckling were taken as $0.34t$ and $0.94t$, respectively, corresponding to a
309 Cumulative Distribution Function (CDF) value of 50%. For specimens with a thickness (t)
310 larger than 3 mm, the imperfection magnitude was determined using the following equation
311 proposed by Walker [45]:

$$\omega_d = 0.3t \sqrt{\frac{\sigma_{0.2\%}}{\sigma_{cr}}} = 0.3t\lambda_s \quad (21)$$

312 where $\sigma_{0.2\%}$ and σ_{cr} are 0.2% proof stress of the material and elastic critical local/distortional
313 buckling stress of the cross-section; respectively, and λ_s is the cross-sectional slenderness,
314 given by:

$$\lambda_s = \sqrt{f_y / \sigma_{cr}} \quad (22)$$

315 The amplitude of geometric imperfection for global buckling, which is in the shape of a
316 half-sine wave, was taken as $L_e / 1500$, as reported in previous studies [31, 46] (where L_e is
317 the length of the member). While local and/or distortional buckling modes were identified to
318 be dominant for the short elements [31], a combination of three buckling modes (i.e. local,
319 distortional and global) was introduced for the medium and long length members [39].

320 *3.4 Validation of the FE models*

321 To predict the capacity of the CFS elements, nonlinear inelastic post-buckling analysis
322 was performed by using the standard RIKS arc-length method in ABAQUS [34]. Table. 1 lists
323 the strength of the CFS column members under pure axial compression obtained from FE
324 models (P_{FE}) and the tests (P_{Test}) [38] for three various lengths (1000, 1500 and 2000 mm)
325 and four different cross-sectional dimensions (A, B, C and D), as shown in Fig. 6(a). Similarly,
326 Table. 2 compares the strength obtained from FE and the tests for CFS beam-column members
327 with three various element lengths (305, 610 and 1219 mm) subjected to compressive loads
328 with nine different eccentricity values on the minor (y) and major axes (x). The beam-column
329 members were consequently subjected to the combined actions of (i) compression and minor
330 axis bending moment, (ii) compression and major axis bending moment and (iii) compression
331 and biaxial bending moments. The cross-sectional dimensions of these beam-column
332 specimens are shown in Fig. 6(b). It should be noted that all demonstrated dimensions are
333 reported out-to-out dimensions.

334 In general, good agreements were achieved between the strength and failure mechanism
335 of the FE models and the corresponding experimental tests. The results demonstrated that the
336 developed FE models could accurately predict the strength of the column and beam-column
337 elements with maximum estimation errors of 8% and 4% with the standard deviations of 0.05
338 and 0.02, respectively. For instance, Figs. 7 and 8 demonstrate that the failure modes predicted
339 by the developed FE models compare very well with those observed during the experimental
340 tests on A1000-a (column element) under axial load and S600-1219-15 (beam-column element)
341 under combined compression and bi-axial bending moments. These two elements failed in local
342 buckling first, followed by the interaction of local and overall flexural buckling about the minor
343 axis. In addition, Fig. 9 compares the axial force-displacement relationship for A1000-a and
344 S600-610-8 specimens obtained from the reference experimental tests and the predicted results
345 from the numerical study. It is demonstrated that the proposed FE models were able to capture
346 the peak load, initial stiffness and post-buckling behaviour of both column and beam-column
347 specimens.

348 **4 Parametric study**

349 The experimentally validated FE models described in the previous section have then been
350 used to conduct a comprehensive parametric study. The purpose of the parametric study is to
351 investigate the effects of warping-restrained boundary conditions on the maximum capacity of
352 CFS structural elements (i.e., columns and beam-columns) and assess the efficiency of the code
353 proposed compression force-bending moment interaction equation as well as the limitations of
354 the current design methods.

355 In total, 270 CFS elements subjected to 10 different load combinations were selected by
356 considering various key design parameters, including three sets of cross-sectional dimensions
357 (*C1*, *C2* and *C3*), thicknesses (1 mm, 2 mm and 4 mm) and lengths (500 mm (short), 1500 mm

358 (medium) and 3000 mm (long)), as shown in Table. 3. The same modelling techniques
359 described in Section 3 were adopted for the parametric study. For a fair comparison, similar
360 material properties were considered for CFS column and beam-column elements ($E = 207$ GPa,
361 $F_y = 350$ MPa, $F_u = 600$ MPa and Poisson ratio = 0.3). Fig. 5(c) demonstrates the bi-linear
362 stress-strain curve used in FE models. The selection of loading conditions was on the basis that
363 the effects of all possible combinations of axial compression force and bending moments can
364 be investigated, including pure compression, combined compression and major axis bending,
365 combined compression and minor axis bending and combined compression and bi-axial
366 bending. This was provided using different values of eccentricities as listed in Table. 4. The
367 failure modes of the selected cross-sections under pure actions are listed in Table. 5, which can
368 be either local, distortional, local-global and yielding. As specified in Eq. 4, the yielding failure
369 in the members subjected to pure bending can be achieved when the calculated elastic critical
370 lateral-torsional moment (M_{cre}) is greater than 2.78 times yield moment (M_y). It should be
371 noted that the dominant failure mode of CFS beam-column members was assumed to be the
372 same as the elements under pure compression, where the dominant mode was determined using
373 the lowest values of the buckling loads obtained from DSM equations (see Section 2). This
374 assumption is generally valid for beam-column elements where the axial behaviour is dominant
375 (which is the case for the specimens considered in this study).

376 **5 Results and discussions**

377 Tables. A1 to A3 in the Appendix A present the strength results of the beam-column
378 members with three different cross-sections ($C1$, $C2$ and $C3$) obtained from the detailed FE
379 models (P_{DFE}) and the four different design methods specified in Section 2, including DSM
380 (P_{DSM}), DSM with warping-restrained elastic buckling resistance ($P_{DSM,W}$), Moen
381 ($P_{Distortional,W}$) [23] and Torabian et al. ($P_{Interaction}$) [39]. These tables also list the values of

382 imposed eccentricities in y (e_y) and x (e_x) directions that generate bending moments about
383 major and minor axes, respectively, ratios of strength predictions obtained from each design
384 method to the detailed FE models, and the calculated statistical indicators.

385 *5.1 Efficiency of the existing design methods*

386 Fig. 10 is used to assess the efficiency of the existing design methods, where average
387 estimation errors in the estimated capacity using the existing design methods in comparison
388 with the detailed FE models are presented under various loading conditions (pure compression,
389 combined compression and minor axis bending with the web in tension or compression,
390 combined compression and major axis bending and combined compression and bi-axial
391 bending). Overall, using existing design methods for the strength calculations of the short CFS
392 member (i.e., 500 mm) results in less accurate predictions compared to medium (i.e., 1500 mm)
393 and long members (i.e., 3000 mm) under combined actions. On the other hand, it is shown that
394 the average ratio of the strength predictions obtained from different design methods and the
395 detailed FE models for the CFS elements under pure compression is 0.87, 0.84 and 0.69 for
396 short, medium, and long length members, respectively. The results also indicate that the DSM
397 led to the most conservative predictions, especially for short members, underestimating the
398 capacity results up to 55% compared to the detailed FE results. This can be attributed to (i) the
399 absence of the warping restrained boundary condition effects, (ii) the DSM equations for the
400 calculations of buckling loads, and (iii) the AISI S100 (2016) [21] linear interaction equation.
401 Based on the results, it can be concluded that the highest estimation error in DSM predictions
402 was observed when the CFS beam-columns were under combined compression and bi-axial
403 bending moments (average estimation errors of 40%, 27% and 19% for short, medium, and
404 long length members, respectively).

405 With respect to the DSM with warping-restrained elastic buckling resistance ($P_{DSM,W}$), it
406 can be clearly seen that this method provided a better prediction than the DSM in all the three
407 selected lengths (by up to 7.3%), arising to the existence of the warping restrained effect in this
408 method as shown in Fig. 10. However, the maximum difference between the predictions of this
409 method and the detailed FE results was still 51% (see Table. A1), which can be attributed to
410 the estimation errors sourcing from the DSM equations and the AISI S100 (2016) [21]
411 interaction equation as discussed before. This highlights the need for further investigations in
412 this area.

413 The method proposed by Moen [23], in which the effects of the end boundary conditions
414 are taken into account for the specimens failing in distortional buckling mode, could provide
415 more accurate strength predictions compared to the DSM by up to 16%. It should be noted that
416 in this study only five cross-sections of the short members were prone to the distortional
417 buckling mode (*C1* with 1-, 2- and 4-mm thickness, and *C2* and *C3* with 4 mm thickness), as
418 shown in Table. 5. Therefore, the efficiency of Moen's method can be solely seen in Fig. 10(a)
419 for the short members (i.e., 500 mm), and the results of the DSM and this method are identical
420 for the medium and long length members (see Fig. 10(b) and (c)). Furthermore, the efficiency
421 of the method proposed by Moen [23] was especially evident in the members with a thickness
422 of 4 mm. In general, the average ratio of strength values obtained from Moen method
423 ($P_{Distortional,W}$) and detailed FE results (P_{DFE}) is 0.71. This average ratio reaches 0.69 when
424 the DSM procedures are used, which indicates the Moen's method provides slightly more
425 accurate capacity predictions. The results also demonstrated that the best agreement between
426 the results of this method and the detailed FE predictions was obtained when members were
427 subjected to the pure compression load. This can be justified considering that this method was
428 originally developed for members under pure compression load.

429 It can be seen that compared to the other design methods, the Torabian et al. method [39]
430 is capable of predicting strength values with a higher level of efficiency in most cases. This is
431 especially evident for the medium length elements, where the load-carrying capacities
432 predicted by this design method are in a reasonable agreement with the detailed FE results with
433 an average underestimated result of 11% (see Fig. 10(b)). In contrast, the most significant
434 estimation error was found in CFS elements with 500 mm length with an average of 25% (see
435 Fig. 10(a)). Fig. 10 also indicates that Torabian et al. method [39] led to better strength
436 predictions when the CFS members are subjected to the combined axial compression and minor
437 axis bending and combined axial compression and bi-axial bending. It should be noted that this
438 method noticeably overestimated the capacities of some of the CFS members, especially those
439 with longer (i.e., 3000 mm) and thicker (i.e., 4 mm) elements (see Tables. A2 and A3).

440 *5.2 Effects of warping-restrained boundary conditions*

441 In order to assess the effects of warping restrained boundary conditions on the capacities
442 of the CFS members, the results of the DSM ignoring the warping-fixed effect and the DSM
443 with warping-restrained elastic buckling resistance are compared in this section. The results
444 demonstrate that restraining warping of CFS elements improved the capacities of the members
445 in all cases (on average by 6%, 2.5% and 1.2% for short, medium and long members), as shown
446 in Fig. 11. It can be noted that while the warping-restrained boundary conditions were more
447 effective for the short CFS elements (see Fig. 11(a)), increasing the element length
448 considerably reduced the effects of warping (see Fig. 11(b) and (c)). This is attributed to the
449 shortening of the buckling half-wavelength caused by the warping-restrained condition, which
450 means the wavelength shortening can be distributed over multiple half-waves as the length of
451 the cross-section increases [23].

452 In general, it can be concluded that the effects of the warping-restrained on the capacity
453 of CFS elements under combined actions were not significant (less than 7.3%). This indicates
454 that the estimation errors associated with the DSM can be referred to the inefficiency of the
455 AISI S100 (2016) interaction equation [21]. On the other hand, when the CFS elements were
456 under pure axial compression, in the absence of the interaction equation, DSM still predicted
457 the strength with a noticeable estimation error (see Fig. 11). This highlights again the
458 estimation error caused by the DSM equations for the cross-sectional buckling capacities. In
459 particular, the most significant estimation error of DMS was observed for the long length
460 members (i.e., 3000 mm) under pure axial compression (31% on average), in which unlike
461 medium and short length members, local-global buckling was determined as the dominant
462 buckling mode (see Table. 5). This is consistent with the results previously reported by Ye et
463 al. [38] that the DSM takes into account the effects of the local-global buckling mode with a
464 noticeable difference.

465 *5.3 Efficiency of the interaction equation*

466 This section investigates the efficiency of the interaction equation proposed by the AISI
467 S100 (2016) [21] for the members under the combined actions of axial compression load and
468 bending moments. To assess the efficiency of the interaction equation, the effects of the
469 warping-restrained boundary conditions and the inaccuracy of the DSM equations should be
470 somehow removed from the results. To this end, the estimation errors of the DSM with
471 warping-restrained elastic buckling resistances for the CFS elements under combined actions
472 were scaled to those for the pure axial compression, as shown in Fig. 12. It should be mentioned
473 that the average errors for combined actions and pure compression were individually obtained
474 by taking the ratios of $\left(\frac{P_{DSM,W}}{P_{DFE}}\right)$ for combined actions and pure compression, respectively. In
475 general, it can be seen that the code suggested interaction equation was more efficient for the

476 medium length beam-column members with an average of 4% error; however, this value
477 reached 19% and 22% for the short and long length elements, respectively. Therefore, it can
478 be concluded that the effects of the interaction equation are more considerable than the effects
479 of the warping-restrained boundary conditions on the accuracy of the strength predictions.
480 Furthermore, the results showed that the influence of the interaction equation on the total
481 estimation error was more evident in the CFS members under combined compression and bi-
482 axial bending moments, especially for short and medium length elements, as shown in Fig. 12.

483 The presented results, in general, highlight the need to develop more efficient interaction
484 equations to design CFS beam-column elements under compression load and bending
485 moments. Besides, more accurate methods are required to take into account the warping
486 restrained boundary condition on the capacity predictions. This is especially important in the
487 case CFS elements are used in moment resisting frame systems where the connections could
488 provide warping fixity. It is also worth noting that DSM equations for long members, in which
489 local-global buckling are determined as the dominant buckling mode, require some
490 modifications to be more efficient.

491 **6 Summary and conclusions**

492 This paper assessed the accuracy of the existing methods in estimating the load-carrying
493 capacity of CFS beam-column members as well as the effects of the warping restrained
494 boundary condition and the efficiency of the interaction equation proposed by AISI S100
495 (2016) [21]. Detailed FE models were developed in ABAQUS by considering the effects of the
496 material nonlinearity and geometric imperfections and validated against the results of two
497 different experimental investigations on CFS lipped channel cross-sections under pure axial
498 compression, compression and minor axis bending moment, compression and major axis
499 bending moment, and compression and biaxial bending moments. A comprehensive parametric

500 study was then conducted using the validated models, covering different cross-sections,
501 lengths, and levels of load eccentricities. A total of 270 FE models were undertaken to compare
502 their results with the current design methods in design guidelines and literature.

503 The accuracy of the existing design methods was compared with the detailed FE models.
504 In general, less accurate load bearing capacity predictions were observed for short length CFS
505 members (i.e., 500 mm) compared to the medium (i.e., 1500 mm) and long length elements
506 (i.e., 3000 mm) under combined actions.

507 Compared to the other methods, the DSM provided the most conservative predictions (up
508 to 55% lower than the detailed FE results), which can be attributed to errors associated with (i)
509 warping restrained boundary condition effects, (ii) the DSM equations for the calculations of
510 buckling loads, and (iii) the AISI linear interaction equation. The maximum error in DSM
511 capacity predictions was seen when the CFS members were subjected to combined
512 compression and bi-axial bending moments (average errors of 40%, 27% and 19% for short,
513 medium and long length members).

514 The DSM with warping-restrained elastic buckling resistance (DSM,W) provided better
515 predictions compared to the conventional DSM by up to 7.3%, while its efficiency was more
516 evident in the shortest length elements. However, the maximum difference between the
517 predictions of this method and the detailed FE results was still 51%.

518 The results of the proposed method by Moen [23] indicated a good agreement with the
519 detailed FE models when the dominant failure mode under pure axial load was the distortional
520 buckling mode (generally the case for short members). For these elements, this method could
521 provide more accurate strength predictions compared to the DSM by up to 16%. However, for
522 the other elements, the results of the DSM and the Moen's proposed method are identical.

523 While the method proposed by Torabian et al. [39] generally provided overestimated
524 results compared to the detailed FE models, it led to more accurate predictions than the other
525 design methods in most cases. A good agreement was observed with the FE models in the
526 intermediate cross-sections (11% error on average); however, there was a considerable
527 difference in the short specimens (25% error on average).

528 It was shown that considering the warping-fixed effect could on average improve the
529 accuracy of the capacity predictions by 6%, 2.5% and 1.2% in short, medium, and long length
530 specimens, respectively. It was demonstrated that increasing the element length reduces the
531 effects of warping, which is attributed to the shortening of the buckling half-wavelength caused
532 by the warping-restrained condition.

533 There was a noticeable estimation error (around 30% on average) between the results of
534 the detailed FE and the current design methods based on DSM in the long CFS members under
535 pure axial compression. The existence of such error, in the absence of interaction effect, can
536 be referred to as the error caused by the DSM equations in which local-global buckling was
537 determined as the dominant buckling mode.

538 The assessment of the interaction equation proposed by the AISI S100 (2016) [21] for
539 the members under the combined actions of compression load and bending moments indicated
540 the better efficiency of this method for the medium length beam-column members with an
541 average of 4% error in the capacity predictions; however, this error increased to 19% and 22%
542 for the short and long length elements, respectively. It can be concluded that the effects of the
543 interaction equation on the accuracy of the strength predictions are more considerable than the
544 warping-restrained boundary conditions. Furthermore, the results showed that the influence of
545 the interaction equation on the total estimation error was more evident in the CFS members
546 under combined compression and bi-axial bending moments, especially for short and medium

547 length elements. This effect seems to be less dominant for the elements under the major axis
548 bending moment.

549 **Acknowledgement**

550 The first author would like to thank the University of Auckland for providing a Doctoral
551 Scholarship.

References

- [1] Mojtabaei, Seyed Mohammad, Mohammad Zaman Kabir, Iman Hajirasouliha, and Mina Kargar. "Analytical and experimental study on the seismic performance of cold-formed steel frames." *Journal of Constructional Steel Research* 143 (2018): 18-31.
<https://doi.org/10.1016/j.jcsr.2017.12.013>
- [2] McCrum, Daniel P., Jordan Simon, Michael Grimes, Brian M. Broderick, James BP Lim, and Andrzej M. Wrzesien. "Experimental cyclic performance of cold-formed steel bolted moment resisting frames." *Engineering Structures* 181 (2019): 1-14.
<https://doi.org/10.1016/j.engstruct.2018.11.063>
- [3] Phan, Duoc T., Seyed Mohammad Mojtabaei, Iman Hajirasouliha, Jun Ye, and James BP Lim. "Coupled element and structural level optimisation framework for cold-formed steel frames." *Journal of Constructional Steel Research* 168 (2020): 105867.
<https://doi.org/10.1016/j.jcsr.2019.105867>
- [4] Mojtabaei, Seyed Mohammad, Jurgen Becque, and Iman Hajirasouliha. "Local buckling in cold-formed steel moment-resisting bolted connections: behavior, capacity, and design." *Journal of Structural Engineering* 146, no. 9 (2020): 04020167.
[https://doi.org/10.1061/\(ASCE\)ST.1943-541X.0002730](https://doi.org/10.1061/(ASCE)ST.1943-541X.0002730)
- [5] Mojtabaei, Seyed Mohammad, Jurgen Becque, and Iman Hajirasouliha. "Behavior and Design of Cold-Formed Steel Bolted Connections Subjected to Combined Actions." *Journal of Structural Engineering* 147, no. 4 (2021): 04021013.
[https://doi.org/10.1061/\(ASCE\)ST.1943-541X.0002966](https://doi.org/10.1061/(ASCE)ST.1943-541X.0002966)
- [6] Papargyriou, Ioannis, and Iman Hajirasouliha. "More efficient design of CFS strap-braced frames under vertical and seismic loading." *Journal of Constructional Steel Research* 185 (2021): 106886. <https://doi.org/10.1016/j.jcsr.2021.106886>
- [7] Papargyriou, Ioannis, Iman Hajirasouliha, Jurgen Becque, and Kypros Pilakoutas. "Performance-based assessment of CFS strap-braced stud walls under seismic loading." *Journal of Constructional Steel Research* 183 (2021): 106731.
<https://doi.org/10.1016/j.jcsr.2021.106731>
- [8] Torabian, Shahabeddin, and Benjamin W. Schafer. "Development and experimental validation of the Direct Strength Method for cold-formed steel beam-columns." *Journal of Structural Engineering* 144, no. 10 (2018): 04018175.
[https://doi.org/10.1061/\(ASCE\)ST.1943-541X.0002117](https://doi.org/10.1061/(ASCE)ST.1943-541X.0002117)
- [9] Torabian, Shahabeddin, Baofeng Zheng, and Benjamin W. Schafer. "Experimental response of cold-formed steel lipped channel beam-columns." *Thin-walled structures* 89 (2015): 152-168. <https://doi.org/10.1016/j.tws.2014.12.003>
- [10] Torabian, Shahabeddin, David C. Fratamico, and Benjamin W. Schafer. "Experimental response of cold-formed steel Zee-section beam-columns." *Thin-walled structures* 98 (2016): 496-517. <https://doi.org/10.1016/j.tws.2015.10.016>
- [11] AISI (American Iron and Steel Institute). *North American specification for the design of cold-formed steel structural members*. AISI S100-12. Washington, DC: AISI, 2012.

- [12] Cheng, Shan-shan, Boksun Kim, and Long-yuan Li. "Lateral–torsional buckling of cold-formed channel sections subject to combined compression and bending." *Journal of Constructional Steel Research* 80 (2013): 174-180.
<https://doi.org/10.1016/j.jcsr.2012.07.026>
- [13] Ma, Jia-Lin, Tak-Ming Chan, and Ben Young. "Cold-formed high-strength steel rectangular and square hollow sections under combined compression and bending." *Journal of Structural Engineering* 145, no. 12 (2019): 04019154.
[https://doi.org/10.1061/\(ASCE\)ST.1943-541X.0002446](https://doi.org/10.1061/(ASCE)ST.1943-541X.0002446)
- [14] ANSI/AISC (American National Standards Institute of steel Construction). *Specification for structural steel buildings*. ANSI/AISC 360-10. Chicago: AISC, 2010.
- [15] CEN (European Committee for Standardization). *Eurocode 3: Design of steel structures—Part 1–1: General rules and rules for buildings*. Brussels, Belgium: CEN, 2005.
- [16] AS (Australia Standards). *Standards Australia international*. New South Wales, Australia: AS, 1990.
- [17] Li, Qiu-Yun, and Ben Young. "Tests of cold-formed steel built-up open section members under eccentric compressive load." *Journal of Constructional Steel Research* 184 (2021): 106775.
<https://doi.org/10.1016/j.jcsr.2021.106775>
- [18] Wang, Bin, Guillaume L. Bosco, Benoit P. Gilbert, Hong Guan, and Lip H. Teh. "Unconstrained shape optimisation of singly-symmetric and open cold-formed steel beams and beam-columns." *Thin-Walled Structures* 104 (2016): 54-61.
<https://doi.org/10.1016/j.tws.2016.03.007>
- [19] Parastesh, Hossein, Seyed Mohammad Mojtabaei, Hamed Taji, Iman Hajirasouliha, and Alireza Bagheri Sabbagh. "Constrained optimization of anti-symmetric cold-formed steel beam-column sections." *Engineering Structures* 228 (2021): 111452.
<https://doi.org/10.1016/j.engstruct.2020.111452>
- [20] Mojtabaei, Seyed Mohammad, Jurgen Becque, and Iman Hajirasouliha. "Structural Size Optimization of Single and Built-Up Cold-Formed Steel Beam-Column Members." *Journal of Structural Engineering* 147, no. 4 (2021): 04021030.
[https://doi.org/10.1061/\(ASCE\)ST.1943-541X.0002987](https://doi.org/10.1061/(ASCE)ST.1943-541X.0002987)
- [21] AISI (American Iron and Steel Institute). *North American specification for the design of cold-formed steel structural members* (AISI S100-16). Washington, DC: AISI, 2016.
- [22] AS/NZS 4600 (Australian Standard/New Zealand Standard)). *Cold-formed steel structures*. Sydney/Wellington, 2018.
- [23] Moen, Cristopher Dennis. "Direct strength design of cold-formed steel members with perforations." PhD diss., Johns Hopkins University, 2009.
- [24] Rajkannu, J. Sevugan, and S. Arul Jayachandran. "Flexural-torsional buckling strength of thin-walled channel sections with warping restraint." *Journal of Constructional Steel Research* 169 (2020): 106041. <https://doi.org/10.1016/j.jcsr.2020.106041>
- [25] AISI (American Iron and Steel Institute). *Specification for the design of cold-formed steel structural members*. Washington (DC): AISI, 1996.

- [26] North American Specification. *Appendix 1: Design of cold-formed steel structural members using the Direct Strength Method*. In: 2004 supplement to the north American specification for the design of cold-formed steel structures. Washington (DC): American Iron and Steel Institute, 2004.
- [27] EN 1993-1-3. *Eurocode 3: Design of steel structures-Part 1-3: General rules: Supplementary rules for cold-formed members and sheeting*. Brussels: European Committee for Standardization, 2006.
- [28] Schafer, Benjamin W. "The direct strength method of cold-formed steel member design." *Journal of constructional steel research* 64, no. 7-8 (2008): 766-778. <https://doi.org/10.1016/j.jcsr.2008.01.022>
- [29] Schafer, Benjamin W., and Teoman Peköz. "Direct strength prediction of cold-formed steel members using numerical elastic buckling solutions." (1998).
- [30] Fang, Zhiyuan, Krishanu Roy, Jiri Mares, Chiu-Wing Sham, Boshan Chen, and James BP Lim. "Deep learning-based axial capacity prediction for cold-formed steel channel sections using Deep Belief Network." In *Structures*, vol. 33, pp. 2792-2802. Elsevier, 2021. <https://doi.org/10.1016/j.istruc.2021.05.096>
- [31] Ye, Jun, Seyed Mohammad Mojtabaei, and Iman Hajirasouliha. "Local-flexural interactive buckling of standard and optimised cold-formed steel columns." *Journal of constructional steel research* 144 (2018): 106-118. <https://doi.org/10.1016/j.jcsr.2018.01.012>
- [32] Schafer, Benjamin W., CUFSM Version 5.04, Department of Civil Engineering, Johns Hopkins University, 2006. <http://www.ce.jhu.edu/bschafer/cufsm/>.
- [33] Papangelis, J. P., & Hancock, G. J. THIN-WALL—Cross Section Analysis and Finite Strip Buckling Analysis of Thin-Walled Structures—User’s Manual, 1995.
- [34] Abaqus/CAE User's Manual, version 6.23, USA, (2021).
- [35] Phan, Duoc T., Seyed Mohammad Mojtabaei, Iman Hajirasouliha, T. L. Lau, and James BP Lim. "Design and optimization of cold-formed steel sections in bolted moment connections considering bimoment." *Journal of Structural Engineering* 146, no. 8 (2020): 04020153. [https://doi.org/10.1061/\(ASCE\)ST.1943-541X.0002715](https://doi.org/10.1061/(ASCE)ST.1943-541X.0002715)
- [36] Ye, Jun, Jurgen Becque, Iman Hajirasouliha, Seyed Mohammad Mojtabaei, and James BP Lim. "Development of optimum cold-formed steel sections for maximum energy dissipation in uniaxial bending." *Engineering structures* 161 (2018): <https://doi.org/10.1016/j.engstruct.2018.01.070>
- [37] Mojtabaei, Seyed Mohammad, Iman Hajirasouliha, and Jun Ye. "Optimisation of cold-formed steel beams for best seismic performance in bolted moment connections." *Journal of Constructional Steel Research* 181 (2021): 106621. <https://doi.org/10.1016/j.jcsr.2021.106621>
- [38] Ye, Jun, Iman Hajirasouliha, and Jurgen Becque. "Experimental investigation of local-flexural interactive buckling of cold-formed steel channel columns." *Thin-walled structures* 125 (2018): 245-258. <https://doi.org/10.1016/j.tws.2018.01.020>
- [39] Torabian, Shahabeddin, Baofeng Zheng, and B. W. Schafer. "Direct strength prediction of cold-formed steel beam-columns." *Research Rep. RP16-3. Ithaca, NY: American Iron and Steel Institute* (2016).

- [40] Schafer, Benjamin W., and Teoman Peköz. "Computational modeling of cold-formed steel: characterizing geometric imperfections and residual stresses." *Journal of constructional steel research* 47, no. 3 (1998b): 193-210. [https://doi.org/10.1016/S0143-974X\(98\)00007-8](https://doi.org/10.1016/S0143-974X(98)00007-8)
- [41] Schafer, Benjamin William, Zhan Li, and Cristopher Dennis Moen. "Computational modelling of cold-formed steel." *Thin-walled structures* 48, no. 10-11 (2010): 752-762. <https://doi.org/10.1016/j.tws.2010.04.008>
- [42] Yu, Cheng, and Benjamin W. Schafer. "Distortional buckling tests on cold-formed steel beams." *Journal of structural engineering* 132, no. 4 (2006): 515-528. [https://doi.org/10.1061/\(ASCE\)0733-9445\(2006\)132:4\(515\)](https://doi.org/10.1061/(ASCE)0733-9445(2006)132:4(515))
- [43] Schafer, Benjamin W., and Teoman Peköz. "Laterally braced cold-formed steel flexural members with edge stiffened flanges." *Journal of Structural Engineering* 125, no. 2 (1999): 118-127. [https://doi.org/10.1061/\(ASCE\)0733-9445\(1999\)125:2\(118\)](https://doi.org/10.1061/(ASCE)0733-9445(1999)125:2(118))
- [44] MATLAB, (R2020b), MathWorks, Natick, MA, 2020.
- [45] Walker, A. C. (Ed.). (1975). *Design and analysis of cold-formed sections*. John Wiley & Sons.
- [46] Meza Ortiz, Francisco. "The behaviour of cold-formed steel built-up structural members." PhD diss., The University of Sheffield, 2018.

Notation

A	Cross-sectional area
A_g	Gross cross-sectional properties
b	Actual width of the plate in EWM
b_{eff}	Effective width of the plate in EWM
b_f	Flange width of a section
CDF	Cumulative distribution function
CFS	Cold formed steel
d	Depth of section
D_{boost}	Boosting factor for distortional critical buckling load
d_1	Overall depth of lip
DSM	Direct strength method
EWM	Effective width method
E	Young's modulus of elasticity
e_x	Eccentricity in x-direction
e_y	Eccentricity in y-direction
e_z	Eccentricity in z-direction
FE	Finite element

FSM	Finite strip method
f_y	Yield strength of the material
I_1, I_2	Moment of inertia about major and minor axes, respectively
K	Effective length factor
L	Length of a member
L_e	Length of a member
L_{crd}	distortional half-wavelength
M_{crd}	Elastic distortional buckling moment
M_{cre}	Elastic lateral-torsional buckling moment
M_{crl}	Elastic local buckling moment
M_n	Nominal flexural capacity
M_{nd}	Nominal member flexural capacity for distortional buckling
M_{ne}	Nominal member flexural capacity for lateral-torsional buckling
M_{nl}	Nominal member flexural capacity for local buckling
M_x, M_y	Design bending moment around the x-and y-axes, respectively
M_{nx}, M_{ny}	Nominal member moment capacities about the x-and y-axes, respectively
M_1, M_2	Smaller and larger moment at the two ends of the member, respectively
M_{1r}, M_{2r}	Required bending moments around major and minor axis, respectively
P	Design axial force
P_{crd}	Elastic distortional buckling load
P_{cre}	Elastic global buckling stress
P_{crl}	Elastic local buckling load
P_n	Nominal capacity of a member in compression
P_{nd}	Nominal member compression capacity for distortional buckling
P_{ne}	Nominal member compression capacity for flexural, torsional and flexural-torsional buckling
P_{nl}	Nominal member compression capacity for local buckling
P_r	Required axial load
P_y	Nominal yield capacity of a member in compression
$P_{DSM,W}$	Predicted capacity from Nonlinear Elastic Buckling Analysis of ABAQUS
P_{DSM}	Predicted capacity from DSM
$P_{Distortional,W}$	Predicted capacity from Moen's method
P_{DFE}	Predicted capacity from detailed finite element models
$P_{Interaction}$	Predicted capacity from Torabian's method
P_{Test}	Experimental capacity of the reference study
P_{FE}	Maximum axial capacity of our validated FE models
t	Thickness of a channel
w_i, w_e	Warping restraint factors
w_y	Elastic section modulus

y_{c1}, y_{c2}	Distance to the centroidal principal major and minor axes, respectively
Z_y	Elastic section modulus
β	Radial length
θ_{MM}	Azimuth angle
λ_c	Non-dimensional slenderness used to determine P_{ne}
λ_d	Non-dimensional slenderness used to determine P_{nd} and M_{nd}
λ_l	Non-dimensional slenderness used to determine P_{nl} and M_{nl}
λ_s	Cross-sectional slenderness
ϕ_{PM}	Elevation angle,
ϵ_e	Measured engineering strain
ϵ_{true}	True strain
σ_{cr}	Elastic critical local/distortional buckling stress
σ_e	Measured engineering stress
σ_r	Required axial stress
σ_{true}	True stress
$\sigma_{0.2\%}$	Proof stress of the material

List of Tables

Table. 1 Comparison between the strength of CFS elements under pure axial compression obtained from the FE models (P^{FE}) and tests (P^{Test}) [38]

Specimen	Length (mm)	P_{Test} (kN)	P_{FE} (kN)	P_{Test}/P_{FE}
A1000-a	1000	99.8	103.8	0.96
A2000-a	2000	78.4	74.8	1.05
B1000-b	1000	110.3	113.1	0.98
B1500-c	1500.1	106.2	108.8	0.98
C1000-c	999.8	42.7	46.2	0.92
C1500-b	1500.1	35.2	34.1	1.03
D1000-a	1000	109	101.8	1.07
D1500-a	1500	95	90.7	1.05
Average				1.005
Standard deviation				0.05

Table. 2 Comparison between the strength of CFS elements under combined action of axial compression and bending moment obtained from the FE models (P^{FE}) and tests (P^{Test}) [39]

Section name	e_y (mm)	e_x (mm)	P_{Test} (kN)	P_{FE} (kN)	P_{Test}/P_{FE}
S600-305-1	0	-25.4	25.4	25.5	1.00
S600-305-11	-191	0	20.6	20.2	1.02
S600-305-15	-76.2	15.24	25.0	26.1	0.96
S600-610-5	0	15.24	25.0	24.6	1.02
S600-610-8	-76.2	0	34.8	35.5	0.98
S600-610-15	-69.9	-14.2	25.0	25.4	0.98
S600-1219-1	0	-38.1	11.1	11.3	0.98
S600-1219-9	-140	0	23.4	23.0	1.02
S600-1219-15	-63.5	-13	17.6	17.4	1.01
Average					1.00
Standard deviation					0.02

Table. 3 Parametric study variables

Section name	Web (d) (mm)	Flange (b_f) (mm)	Lip (d_1) (mm)	Thickness (t) (mm)	Length (L) (mm)
C1	300	50	25	1	500
				2	1500
				4	3000
C2	250	75	25	1	500
				2	1500
				4	3000
C3	200	100	25	1	500
				2	1500
				4	3000

Table. 4 Magnitude of eccentricities

Loading condition	e_y (mm)	e_x (mm)
Pure compression	0	0
Minor axis bending + compression load	0	10
	0	-25
	0	50
Major axis bending + compression load	10	0
	100	0
	200	0
Bi-axial bending moment + compression load	10	10
	100	-25
	200	50

*Negative sign shows that the lips of the specimens are in tension.

Table. 5 Dominant failure mode of selected cross-sections under pure actions

Cross-section	Length (mm)	Thickness (mm)	Dominant failure modes of cross-sections based on DSM results			
			Compression	Major axis bending	Minor axis bending (web in compression)	Minor axis bending (web in tension)
C1	500	1	Distortional	Local	Yield	Local
		2	Distortional	Local	Yield	Yield
		4	Distortional	Yield	Yield	Yield
	1500	1	Local	Local	Yield	Local
		2	Local	Distortional	Yield	Yield
		4	Local	Local	Yield	Yield
	3000	1	Local	Local	Yield	Local
		2	Local	Local	Yield	Local
		4	Local-Global	Local	Yield	Local & Global
C2	500	1	Local	Local	Yield	Distortional
		2	Local	Distortional	Yield	Distortional
		4	Distortional	Yield	Yield	Yield
	1500	1	Local	Local	Yield	Distortional
		2	Local	Distortional	Yield	Distortional
		4	Local	Yield	Yield	Yield
	3000	1	Local	Local	Yield	Distortional
		2	Local	Local	Yield	Distortional
		4	Local-Global	Local	Yield	Local & Global
C3	500	1	Local	Local	Yield	Distortional
		2	Local	Distortional	Local	Distortional
		4	Distortional	Distortional	Yield	Yield
	1500	1	Local	Local	Yield	Distortional
		2	Local	Distortional	Local	Distortional
		4	Local	Distortional	Yield	Yield
	3000	1	Local	Local	Yield	Distortional
		2	Local	Distortional	Local	Distortional
		4	Local-Global	Local	Yield	Local & Global

List of Figures

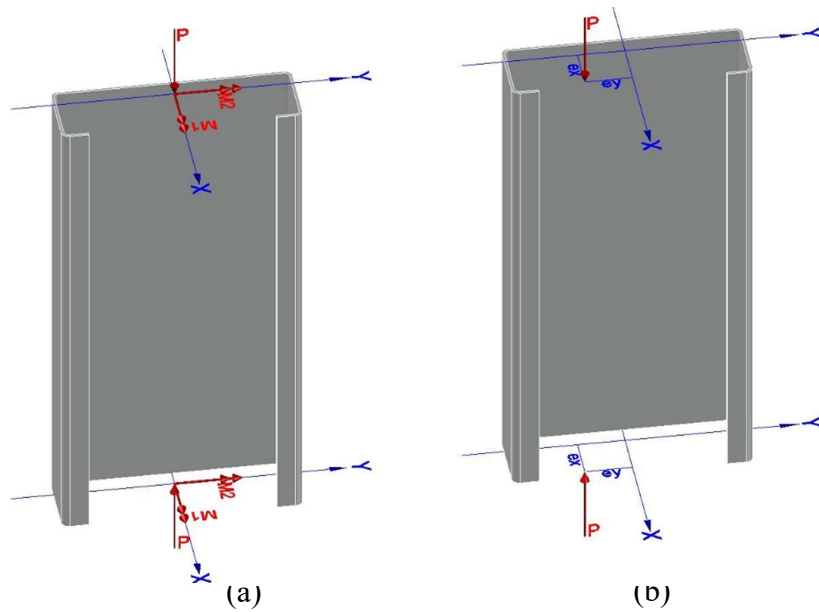


Fig. 1 Beam-column members subjected to (a) combined axial load and bending moment (b) eccentric axial load

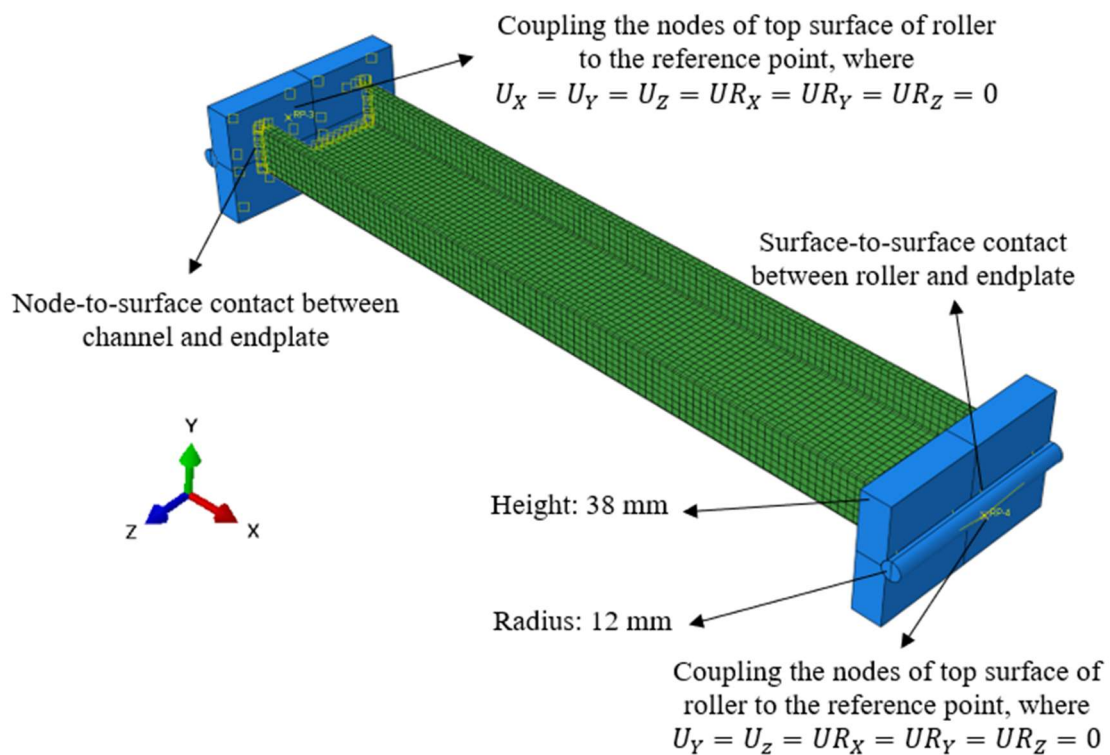


Fig. 2 Boundary conditions of CFS elements under pure axial compressive loads (adopted from Ye et al. [38])

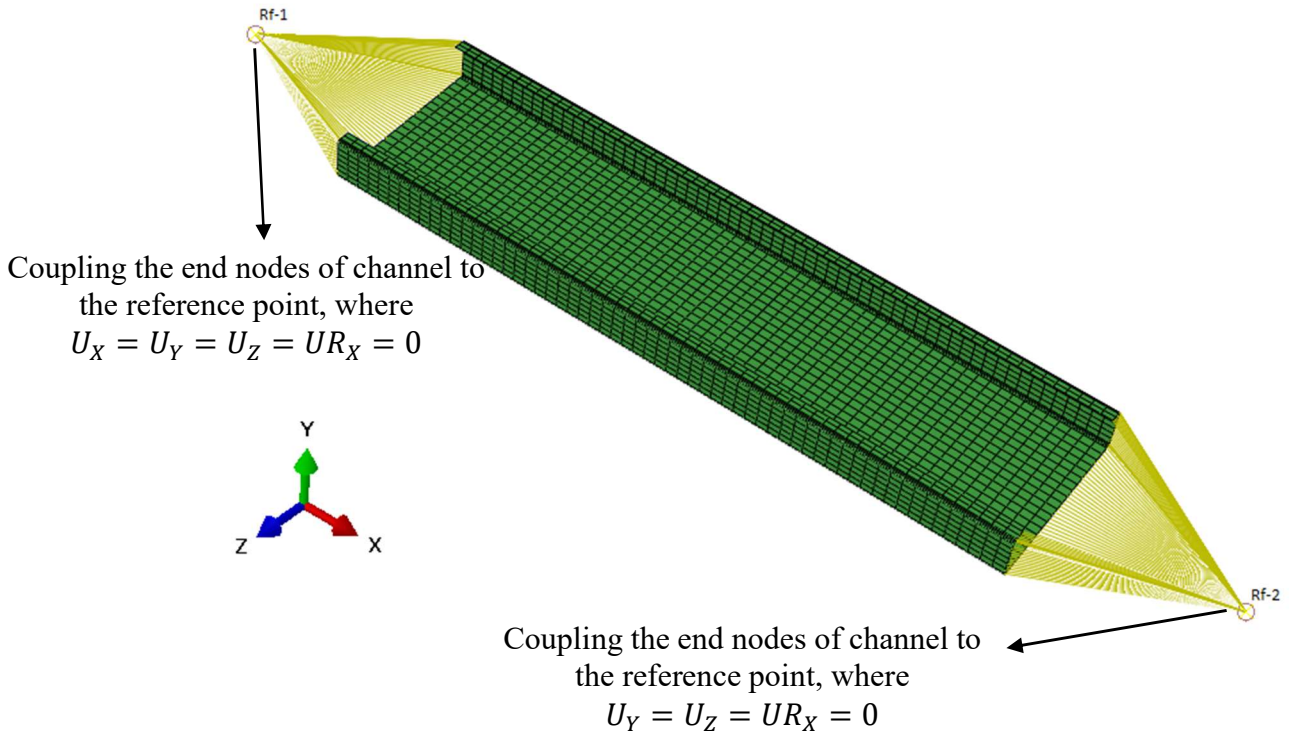


Fig. 3 Boundary conditions of CFS elements under eccentric compressive loads (adopted from Torabian et al. [39])

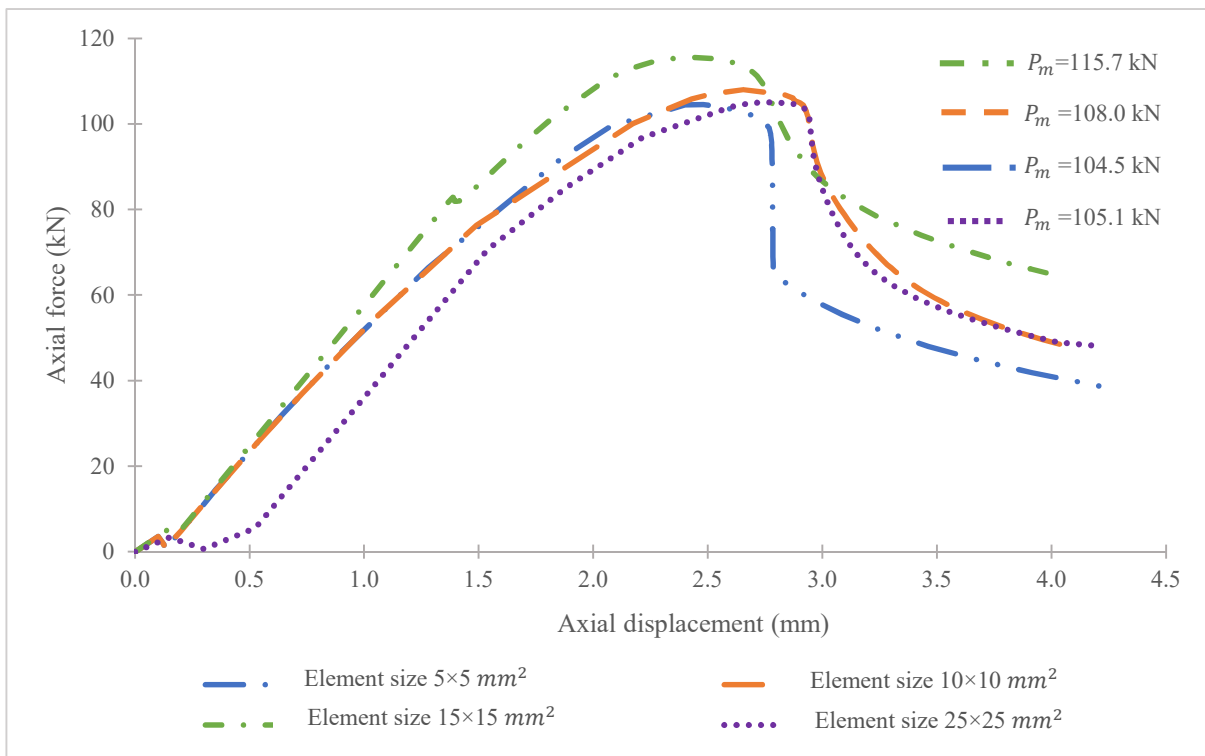


Fig. 4 Axial load vs displacement of B1500-c specimen with various element sizes in flat regions and the number of four elements in corners

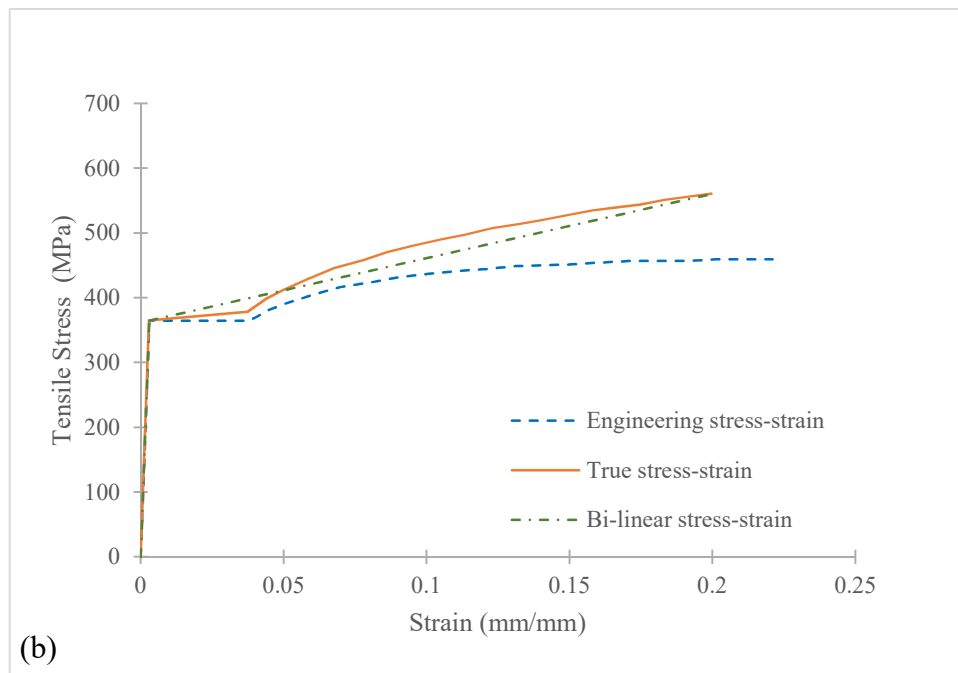
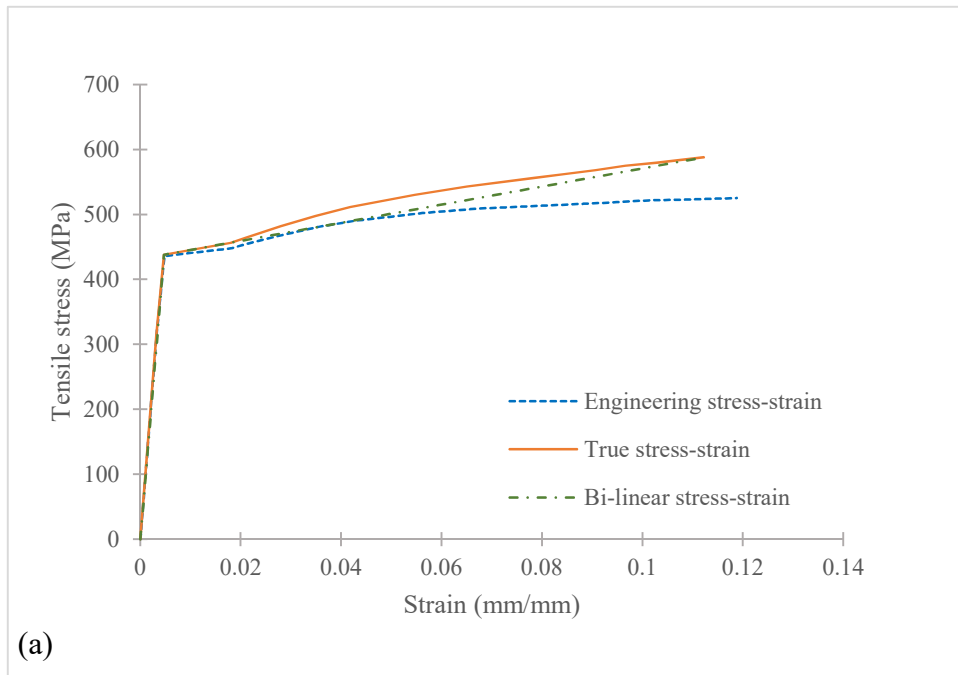


Fig. 5 Stress-strain curves for: (a) columns (Ye et al. [38]) and (b) beam-columns (Torabian et al. [39])

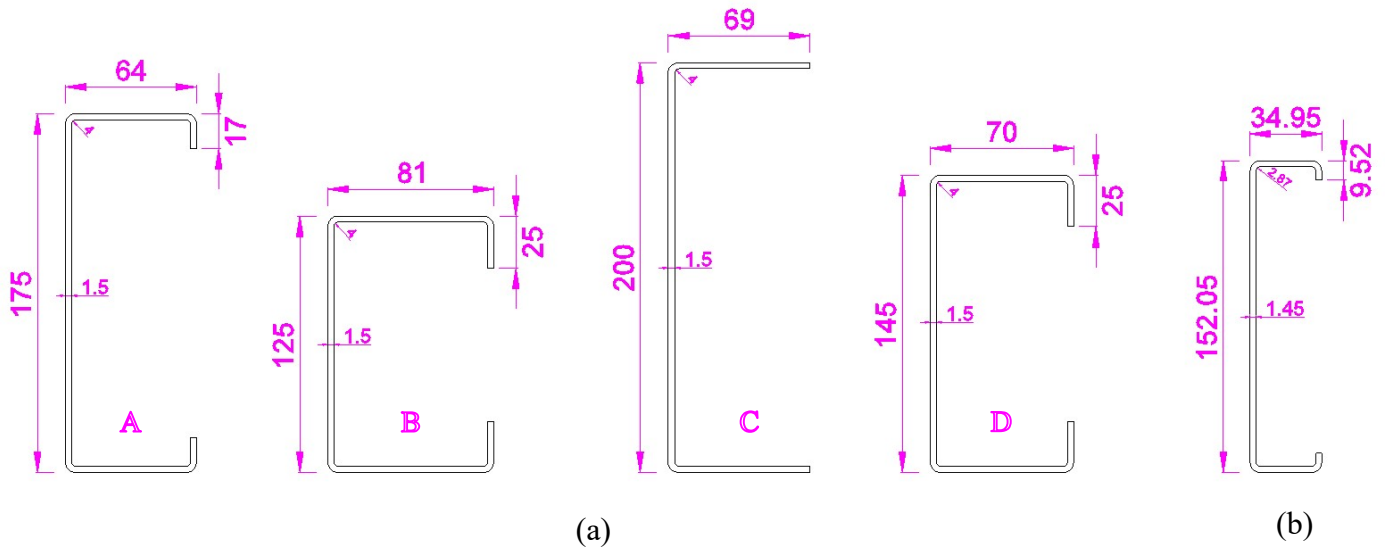


Fig. 6 Cross-sectional geometry of the tested: (a) columns [38] and (b) beam-columns [39]

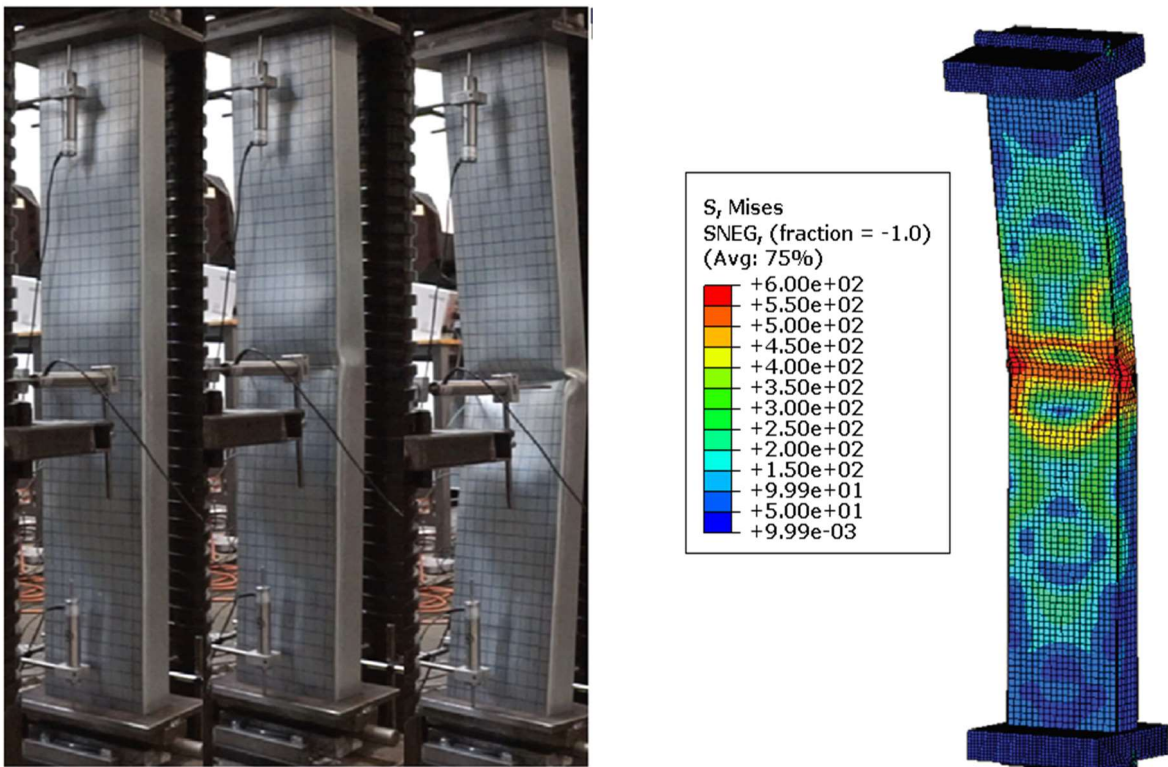


Fig. 7 Failure mode obtained from FE model vs experimental result (A1000-a) (test set-up adopted from Ye et al. [38])

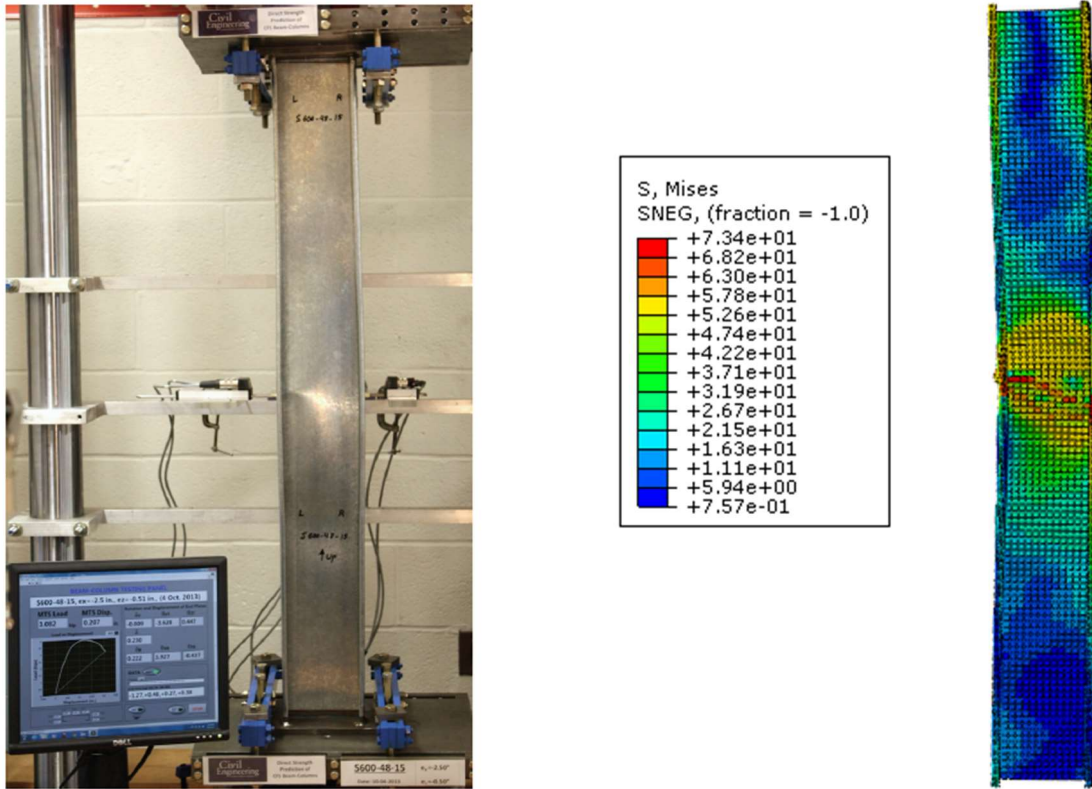
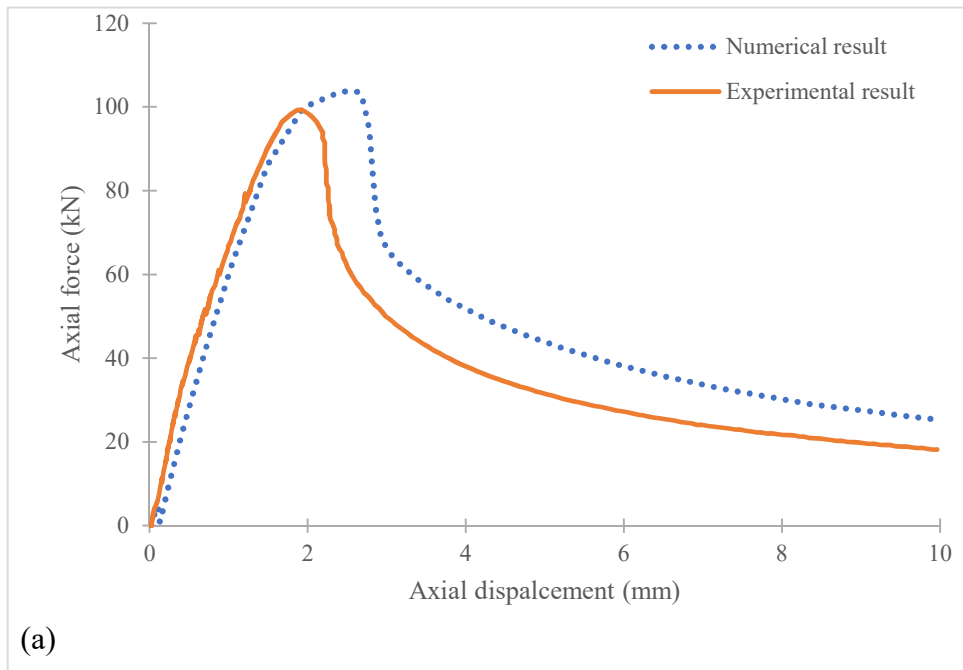


Fig. 8 Failure mode obtained from FE model vs experimental result (S600-1219-15) (test set-up adopted from Torabian et al. [39])



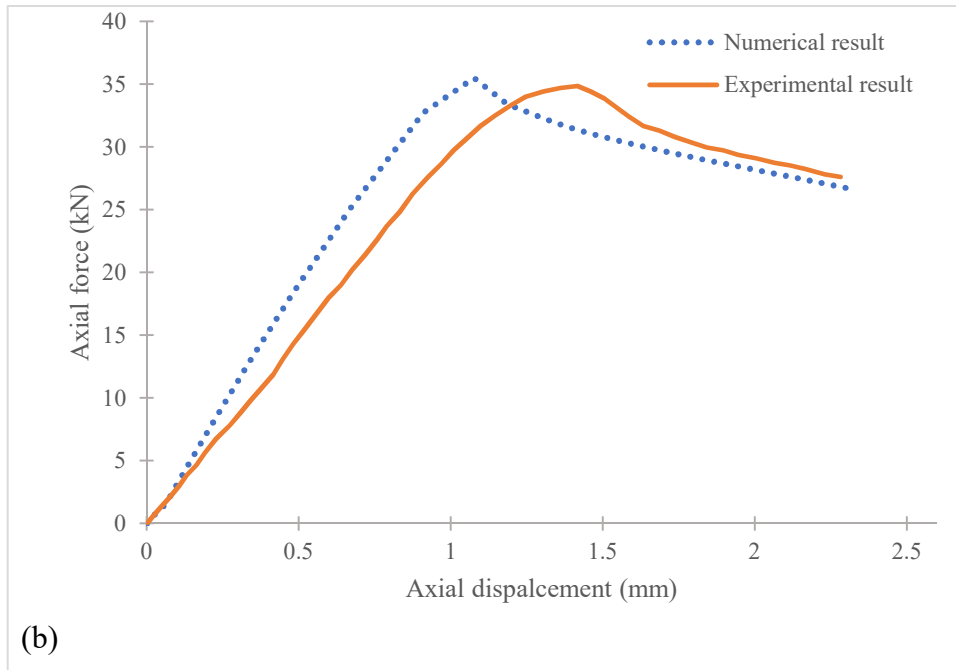
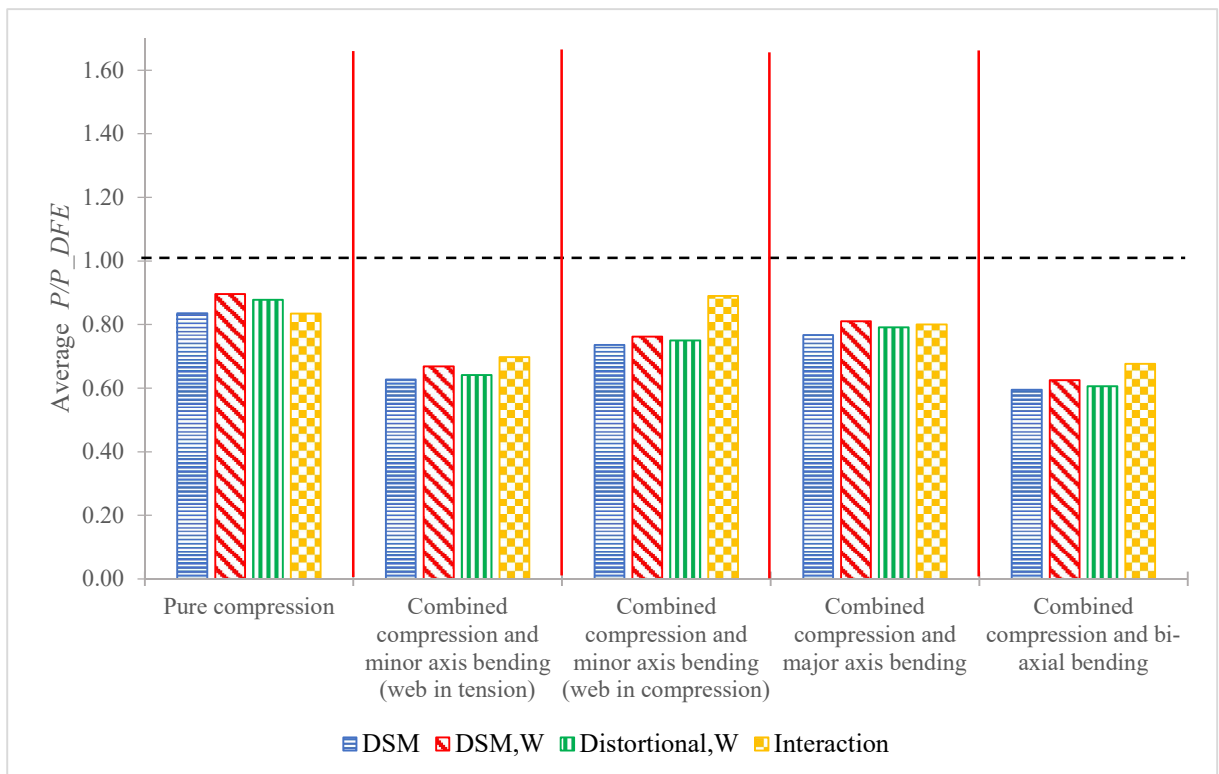
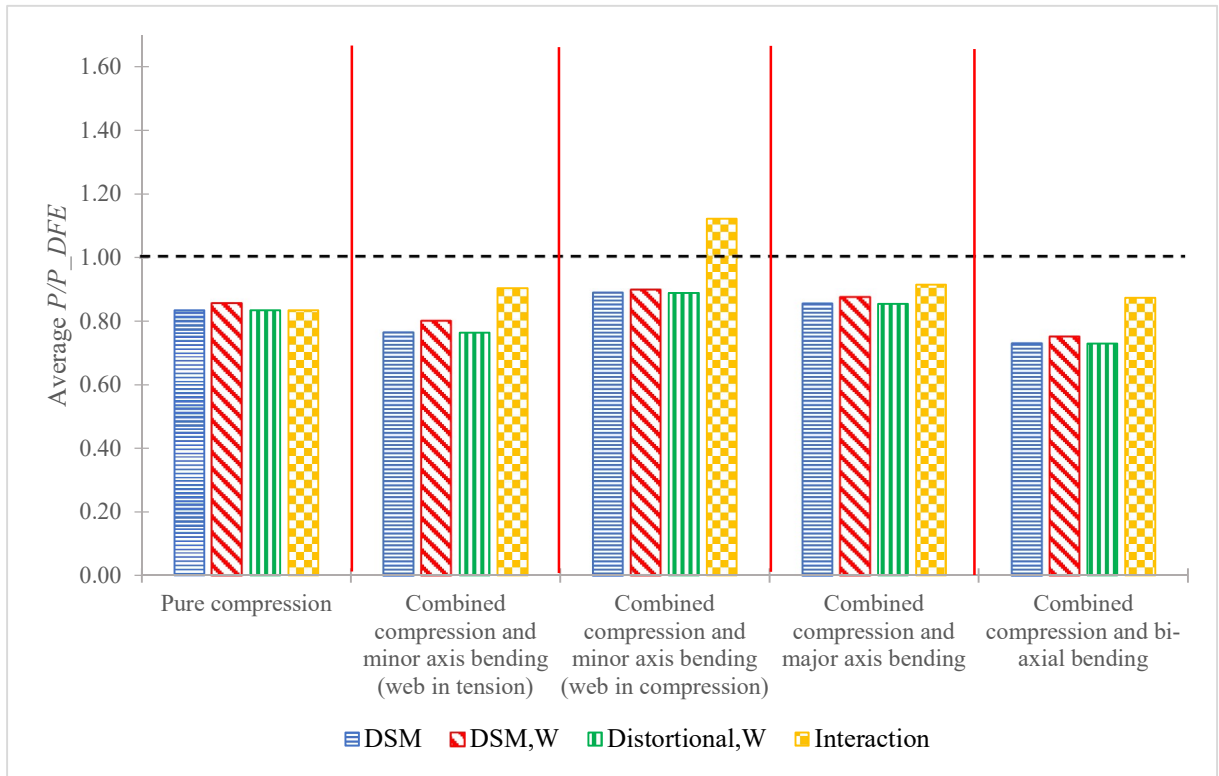


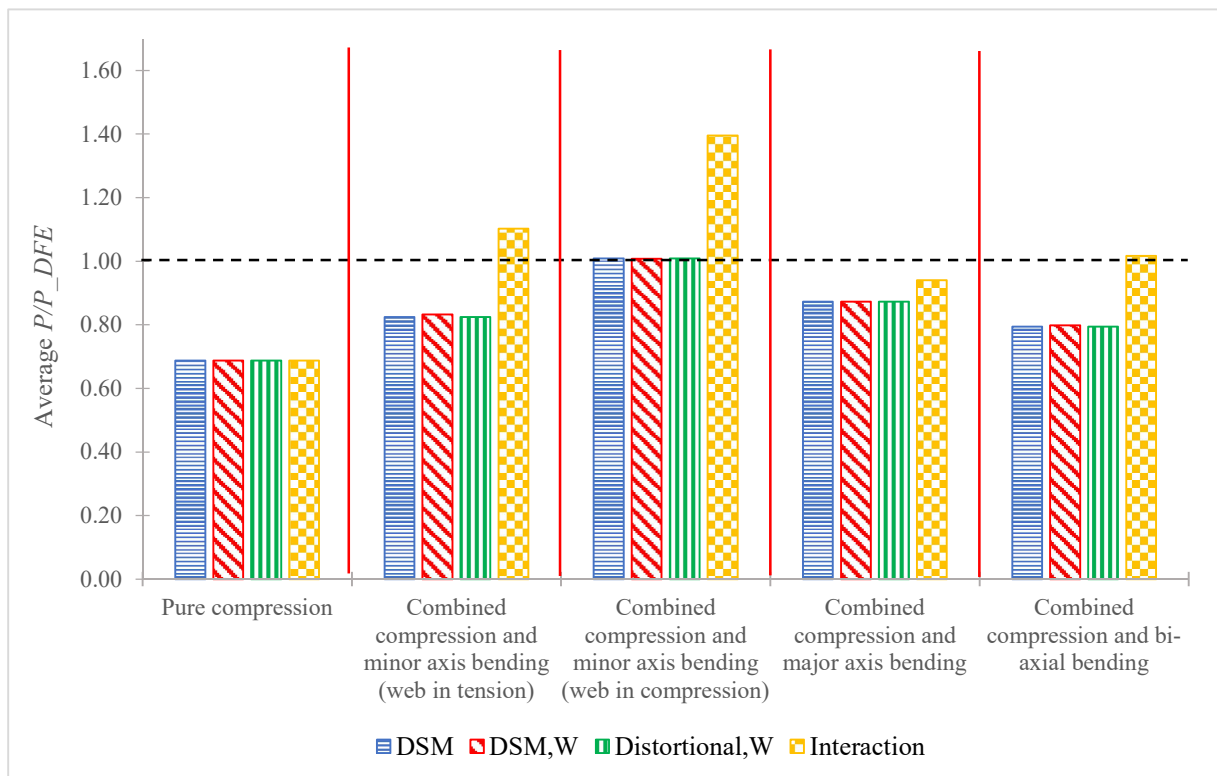
Fig. 9 Axial force-displacement relationship resulting from reference experimental tests against FE (a) A1000-a and (b) S600-610-8



(a) 500 mm

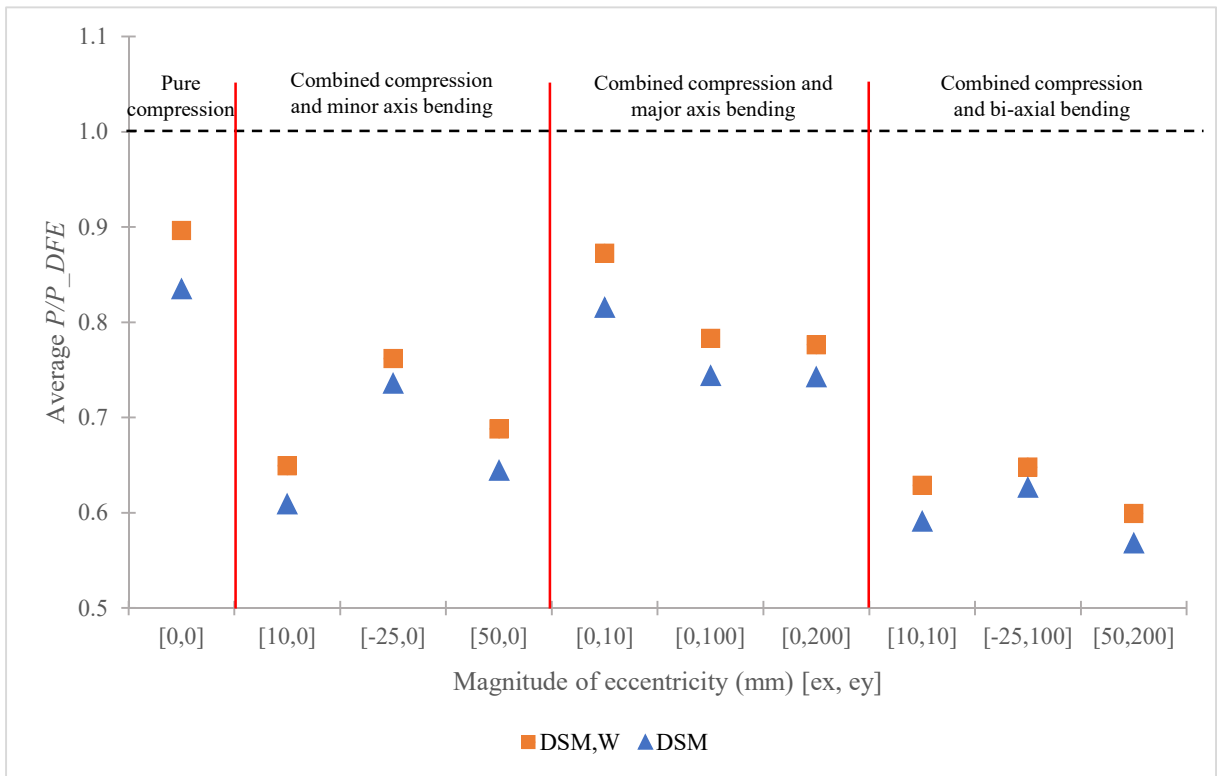


(b) 1500 mm

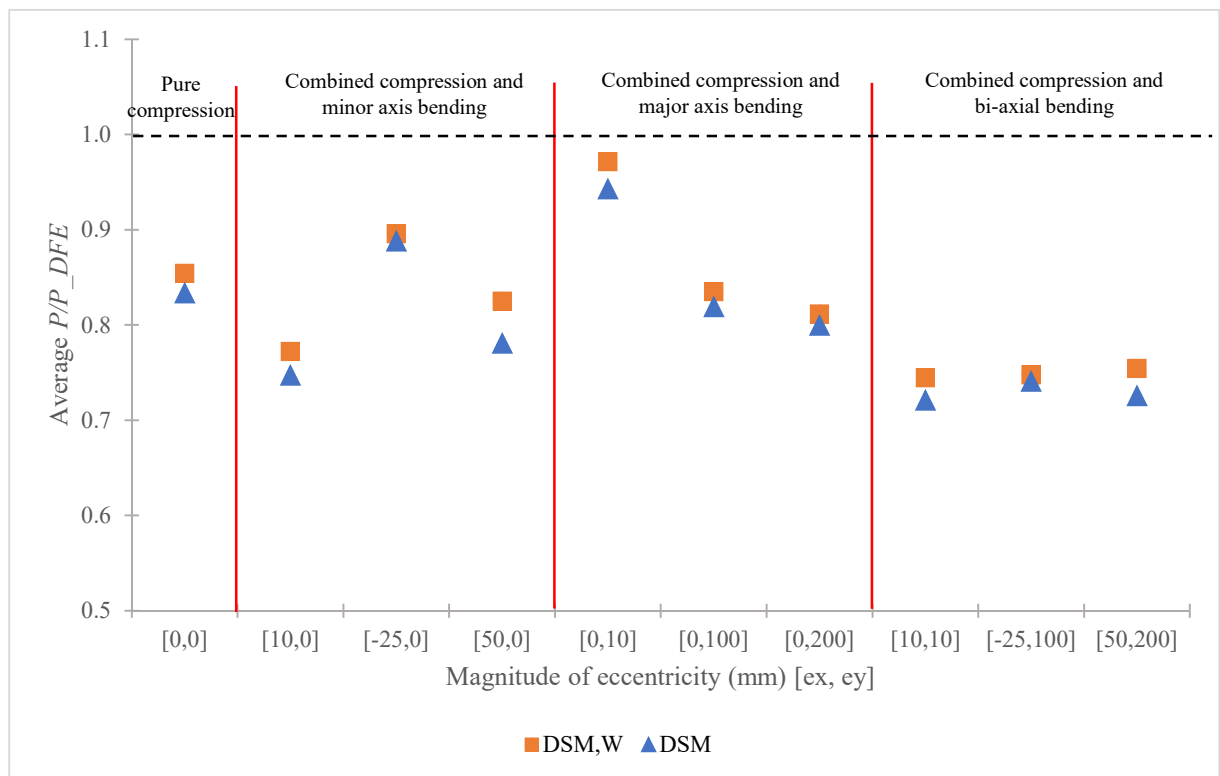


(c) 3000 mm

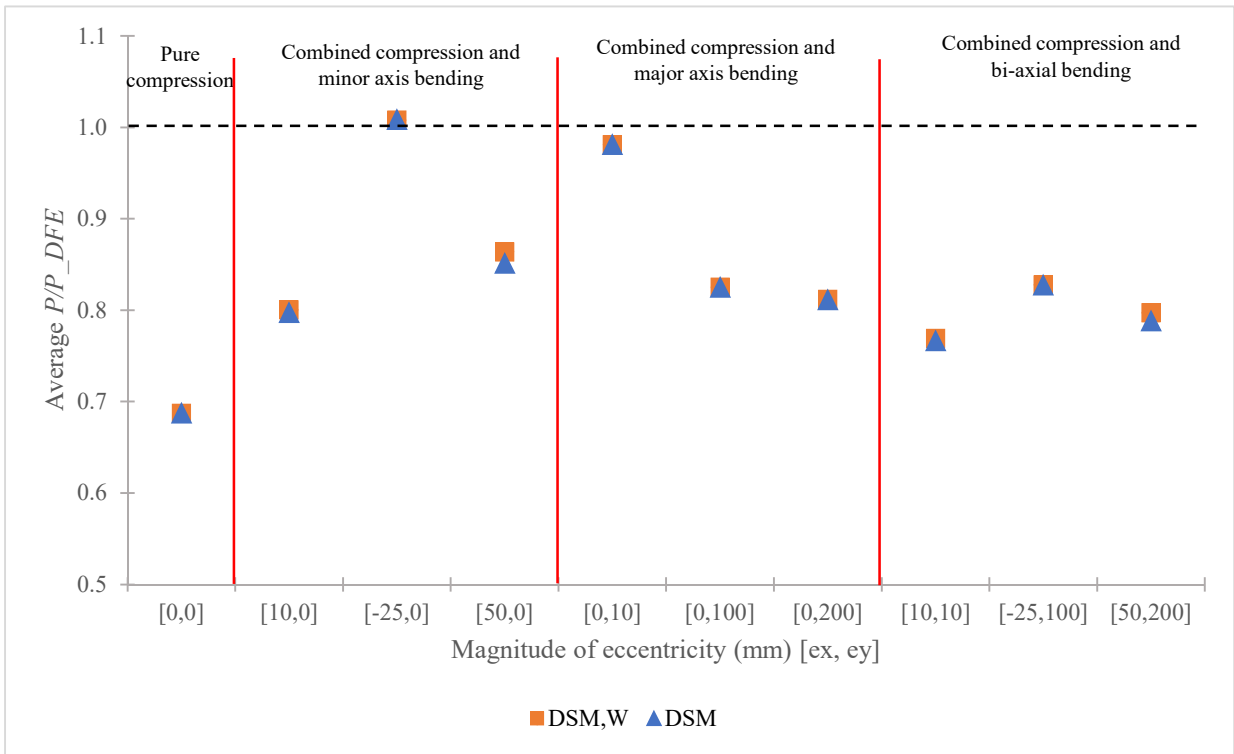
Fig. 10 Average ratios associated with the existing design methods in comparison with the detailed FE models for the strength calculations of CFS elements under various loading conditions



(a) 500 mm



(b) 1500 mm



(c) 3000 mm

Fig. 11 Average ratios associated with the DSM and DSM with warping-restrained elastic buckling resistance in comparison to the detailed FE models for the CFS elements under various eccentricity values

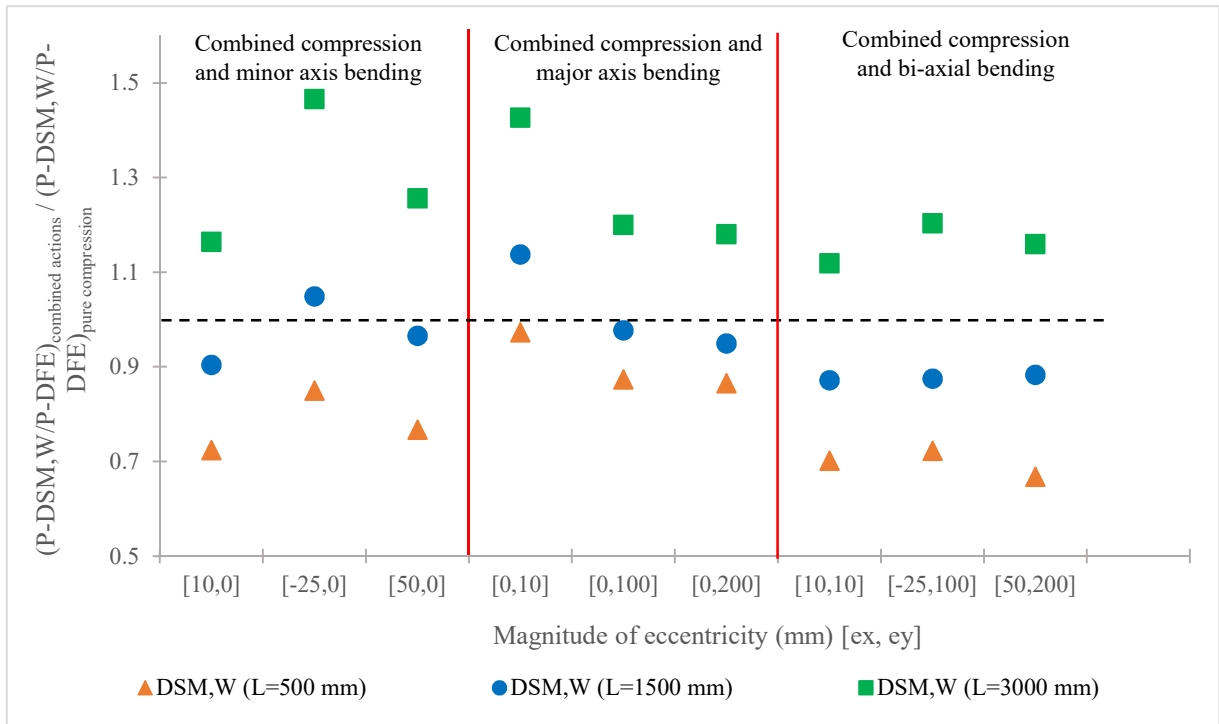


Fig. 12 Average errors associated with the DSM with warping-restrained elastic buckling resistances for the CFS elements under combined actions scaled to those under pure compression

Appendix A

Table. A1 Comparison between the results of strength for the beam-column members with C1 cross-section ($d = 300$ mm, $b_f = 50$ mm, $d_1 = 25$ mm) obtained from detailed FE models and different design methods.

Length L (mm)	Thickness t (mm)	Eccentricity		Capacity					Ratio of each design method prediction to the detailed FE result			
		e_y (mm)	e_x (mm)	P_{DFE} (kN)	P_{DSM} (kN)	$P_{DSM,W}$ (kN)	$P_{Distortional,W}$ (kN)	$P_{Interaction}$ (kN)	$\frac{P_{DSM}}{P_{DFE}}$	$\frac{P_{DSM,W}}{P_{DFE}}$	$\frac{P_{Distortional,W}}{P_{DFE}}$	$\frac{P_{Interaction}}{P_{DFE}}$
500	1	0	0	47.9	36.4	40.5	38.2	36.4	0.76	0.85	0.80	0.76
		0	10	58.2	26.8	29.0	27.7	28.0	0.46	0.50	0.48	0.48
		0	-25	25.0	21.3	22.7	21.9	21.6	0.86	0.91	0.88	0.86
		0	50	17.6	13.0	13.6	13.2	17.4	0.74	0.77	0.75	0.99
		10	0	43.1	34.4	38.0	35.9	35.5	0.80	0.88	0.83	0.82
		100	0	33.5	22.8	24.3	23.4	23.4	0.68	0.73	0.70	0.70
		200	0	25.1	16.6	17.4	16.9	17.0	0.66	0.69	0.67	0.68
		10	10	56.6	25.6	27.7	26.5	27.1	0.45	0.49	0.47	0.48
		100	-25	22.6	15.8	16.5	16.1	15.5	0.70	0.73	0.71	0.69
		200	50	15.7	9.1	9.4	9.2	12.7	0.58	0.60	0.59	0.81
Average				34.51	22.18	23.91	22.91	23.46	0.67	0.71	0.69	0.73
Standard deviation				15.86	8.91	10.15	9.45	8.22	0.14	0.15	0.14	0.16
500	2	0	0	149.6	110.2	123.4	127.3	110.2	0.74	0.82	0.85	0.74
		0	10	141.5	75.6	81.6	83.3	86.2	0.53	0.58	0.59	0.61
		0	-25	76.2	51.4	54.1	54.9	65.1	0.68	0.71	0.72	0.85
		0	50	54.3	33.5	34.7	35.0	41.7	0.62	0.64	0.64	0.77
		10	0	139.1	104.2	116.0	119.4	106.0	0.75	0.83	0.86	0.76
		100	0	106.5	70.2	75.4	76.8	77.0	0.66	0.71	0.72	0.72
		200	0	78.1	51.5	54.3	55.0	55.4	0.66	0.69	0.70	0.71
		10	10	141.1	72.8	78.3	79.9	83.5	0.52	0.56	0.57	0.59

		100	-25	69.1	40.6	42.3	42.7	51.1	0.59	0.61	0.62	0.74
		200	50	48.8	24.9	25.5	25.7	31.1	0.51	0.52	0.53	0.64
Average				100.43	63.50	68.56	69.98	70.73	0.62	0.67	0.68	0.71
Standard deviation				39.65	28.51	32.78	34.04	26.47	0.09	0.11	0.11	0.08
500	4	0	0	426.0	347.3	381.2	405.1	347.3	0.82	0.89	0.95	0.82
		0	10	283.0	190.3	200.0	206.4	230.0	0.67	0.71	0.73	0.81
		0	-25	188.0	113.4	116.7	118.9	223.7	0.60	0.62	0.63	1.19
		0	50	103.3	67.7	68.9	69.7	73.9	0.66	0.67	0.67	0.72
		10	0	392.0	323.4	352.6	372.9	328.3	0.83	0.90	0.95	0.84
		100	0	279.8	199.7	210.5	217.6	216.3	0.71	0.75	0.78	0.77
		200	0	200.0	140.2	145.4	148.7	152.1	0.70	0.73	0.74	0.76
		10	10	282.8	182.9	191.8	197.7	220.2	0.65	0.68	0.70	0.78
		100	-25	168.6	91.3	93.5	94.9	138.1	0.54	0.55	0.56	0.82
		200	50	98.1	52.6	53.3	53.7	56.2	0.54	0.54	0.55	0.57
Average				242.14	170.87	181.40	188.55	198.61	0.67	0.70	0.73	0.81
Standard deviation				111.13	100.54	111.96	120.02	96.01	0.10	0.12	0.14	0.15
1500	1	0	0	34.4	29.0	29.4	29.0	29.0	0.84	0.85	0.84	0.84
		0	10	41.5	22.5	23.9	22.5	26.5	0.54	0.58	0.54	0.64
		0	-25	17.9	18.6	18.7	18.6	19.4	1.04	1.04	1.04	1.08
		0	50	16.5	11.9	13.7	11.9	17.4	0.72	0.83	0.72	1.05
		10	0	28.5	27.6	28.0	27.6	28.5	0.97	0.98	0.97	1.00
		100	0	24.9	19.4	19.5	19.4	20.7	0.78	0.79	0.78	0.83
		200	0	20.4	14.6	14.6	14.6	15.4	0.72	0.72	0.72	0.76
		10	10	40.9	21.7	23.0	21.7	25.6	0.53	0.56	0.53	0.63
		100	-25	16.5	14.1	14.2	14.1	14.9	0.85	0.86	0.85	0.90
		200	50	12.6	8.5	9.3	8.5	12.7	0.67	0.74	0.67	1.01
Average				25.40	18.79	19.44	18.79	21.01	0.77	0.80	0.77	0.87
Standard deviation				10.50	6.66	6.59	6.66	6.01	0.17	0.16	0.17	0.16
1500	2	0	0	110.1	94.8	95.7	94.8	94.8	0.86	0.87	0.86	0.86
		0	10	86.9	68.0	68.5	68.0	85.0	0.78	0.79	0.78	0.98

		0	-25	49.1	47.8	48.0	47.8	66.8	0.97	0.98	0.97	1.36
		0	50	37.7	32.0	32.1	32.0	41.7	0.85	0.85	0.85	1.10
		10	0	82.9	90.2	91.0	90.2	92.4	1.09	1.10	1.09	1.11
		100	0	72.9	62.7	63.1	62.7	67.2	0.86	0.87	0.86	0.92
		200	0	59.5	46.9	47.0	46.9	49.8	0.79	0.79	0.79	0.84
		10	10	86.7	65.6	66.1	65.6	82.2	0.76	0.76	0.76	0.95
		100	-25	45.9	38.0	38.1	38.0	46.2	0.83	0.83	0.83	1.01
		200	50	33.3	23.8	23.8	23.8	31.1	0.71	0.71	0.71	0.93
Average				66.50	56.97	57.35	56.97	65.71	0.85	0.85	0.85	1.01
Standard deviation				25.24	23.65	23.96	23.65	22.65	0.11	0.11	0.11	0.15
1500	4	0	0	336.5	288.0	344.7	288.0	288.0	0.86	1.02	0.86	0.86
		0	10	160.8	171.0	189.4	171.0	226.3	1.06	1.18	1.06	1.41
		0	-25	110.5	106.2	113.1	106.2	177.9	0.96	1.02	0.96	1.61
		0	50	71.5	65.1	67.6	65.1	73.8	0.91	0.95	0.91	1.03
		10	0	209.7	270.2	319.5	270.2	281.6	1.29	1.52	1.29	1.34
		100	0	186.2	173.7	192.8	173.7	203.4	0.93	1.04	0.93	1.09
		200	0	152.2	124.3	133.8	124.3	141.3	0.82	0.88	0.82	0.93
		10	10	160.6	164.5	181.6	164.5	221.8	1.02	1.13	1.02	1.38
		100	-25	105.6	85.5	89.9	85.5	133.5	0.81	0.85	0.81	1.26
		200	50	64.2	50.2	51.7	50.2	55.6	0.78	0.80	0.78	0.87
Average				155.77	149.87	168.40	149.87	180.32	0.94	1.04	0.94	1.18
Standard deviation				79.32	80.70	99.62	80.70	79.46	0.15	0.21	0.15	0.26
3000	1	0	0	18.0	13.7	13.8	13.7	13.7	0.76	0.77	0.76	0.76
		0	10	20.5	12.0	12.0	12.0	17.0	0.58	0.59	0.58	0.83
		0	-25	10.2	10.8	10.9	10.8	11.9	1.06	1.07	1.06	1.16
		0	50	10.8	7.9	7.9	7.9	14.5	0.73	0.73	0.73	1.34
		10	0	13.9	13.2	13.3	13.2	13.7	0.96	0.96	0.96	0.99
		100	0	13.1	10.1	10.1	10.1	10.7	0.77	0.77	0.77	0.82
		200	0	11.7	7.9	7.9	7.9	8.2	0.68	0.68	0.68	0.70
		10	10	20.7	11.6	11.7	11.6	16.6	0.56	0.56	0.56	0.80

		100	-25	9.7	8.4	8.4	8.4	9.4	0.87	0.87	0.87	0.97
		200	50	8.6	5.5	5.6	5.5	9.9	0.64	0.64	0.64	1.15
Average				13.72	10.12	10.16	10.12	12.57	0.76	0.76	0.76	0.95
Standard deviation				4.46	2.64	2.66	2.64	3.02	0.16	0.16	0.16	0.21
3000	2	0	0	61.8	43.0	43.1	43.0	43.0	0.69	0.70	0.69	0.70
		0	10	40.4	35.8	35.9	35.8	52.9	0.89	0.89	0.89	1.31
		0	-25	25.8	29.7	29.8	29.7	37.8	1.15	1.16	1.15	1.47
		0	50	22.8	21.4	21.4	21.4	32.5	0.94	0.94	0.94	1.42
		10	0	35.8	41.4	41.5	41.4	43.1	1.16	1.16	1.16	1.20
		100	0	34.0	31.2	31.3	31.2	33.8	0.92	0.92	0.92	0.99
		200	0	30.1	24.5	24.5	24.5	25.6	0.81	0.82	0.81	0.85
		10	10	40.2	34.7	34.8	34.7	51.9	0.86	0.86	0.86	1.29
		100	-25	24.8	23.6	23.6	23.6	21.2	0.95	0.95	0.95	0.85
		200	50	19.2	15.6	15.6	15.6	21.0	0.81	0.81	0.81	1.09
Average				33.50	30.07	30.16	30.07	36.26	0.92	0.92	0.92	1.12
Standard deviation				12.32	8.88	8.92	8.88	11.59	0.15	0.15	0.15	0.26
3000	4	0	0	153.3	96.2	96.2	96.2	96.2	0.63	0.63	0.63	0.63
		0	10	72.8	77.2	77.2	77.2	107.2	1.06	1.06	1.06	1.47
		0	-25	53.5	61.2	61.2	61.2	109.1	1.14	1.14	1.14	2.04
		0	50	42.7	43.1	43.1	43.1	61.9	1.01	1.01	1.01	1.45
		10	0	77.0	92.3	92.3	92.3	97.3	1.20	1.20	1.20	1.26
		100	0	73.1	67.4	67.4	67.4	74.7	0.92	0.92	0.92	1.02
		200	0	64.9	51.9	51.9	51.9	53.3	0.80	0.80	0.80	0.82
		10	10	72.6	74.7	74.7	74.7	106.2	1.03	1.03	1.03	1.46
		100	-25	52.1	48.1	48.1	48.1	82.1	0.92	0.92	0.92	1.58
		200	50	35.8	31.2	31.2	31.2	40.6	0.87	0.87	0.87	1.13
Average				69.78	64.34	64.34	64.34	82.86	0.96	0.96	0.96	1.29
Standard deviation				32.57	21.23	21.23	21.23	24.44	0.17	0.17	0.17	0.41
Average of all 90 results				82.42	65.19	69.30	67.96	76.84	0.80	0.82	0.81	0.96
Standard deviation of all 90 results				36.78	31.30	35.32	34.14	30.87	0.14	0.15	0.14	0.21

Table. A2 Comparison between the results of strength for the beam-column members with C2 cross-section ($d = 300$ mm, $b_f = 50$ mm, $d_1 = 25$ mm) obtained from detailed FE models and different design methods.

Length	Thickness	Eccentricity		Capacity					Ratio of each design method prediction to the detailed FE result			
				P_{DFE} (kN)	P_{DSM} (kN)	$P_{DSM,W}$ (kN)	$P_{Distortional,W}$ (kN)	$P_{Interaction}$ (kN)	$\frac{P_{DSM}}{P_{DFE}}$	$\frac{P_{DSM,W}}{P_{DFE}}$	$\frac{P_{Distortional,W}}{P_{DFE}}$	$\frac{P_{Interaction}}{P_{DFE}}$
500	1	0	0	52.0	43.8	46.2	43.8	43.8	0.84	0.89	0.84	0.84
		0	10	60.8	34.4	36.5	34.4	35.7	0.57	0.60	0.57	0.59
		0	-25	33.5	29.5	30.6	29.5	26.8	0.88	0.91	0.88	0.80
		0	50	26.5	18.4	19.9	18.4	22.0	0.70	0.75	0.70	0.83
		10	0	49.5	41.0	43.1	41.0	40.7	0.83	0.87	0.83	0.82
		100	0	33.1	26.0	26.9	26.0	25.7	0.79	0.81	0.79	0.78
		200	0	22.8	18.5	18.9	18.5	18.6	0.81	0.83	0.81	0.81
		10	10	57.3	32.6	34.5	32.6	34.1	0.57	0.60	0.57	0.59
		100	-25	26.5	20.2	20.7	20.2	18.5	0.76	0.78	0.76	0.70
		200	50	18.7	11.7	12.3	11.7	14.3	0.63	0.66	0.63	0.77
Average				38.06	27.63	28.96	27.63	28.03	0.74	0.77	0.74	0.75
Standard deviation				15.40	10.51	11.16	10.51	10.09	0.12	0.12	0.12	0.10
500	2	0	0	185.5	146.2	153.8	146.2	146.2	0.79	0.83	0.79	0.79
		0	10	205.2	106.7	113.3	106.7	116.3	0.52	0.55	0.52	0.57
		0	-25	109.5	79.1	81.3	79.1	88.3	0.72	0.74	0.72	0.81
		0	50	91.1	51.3	55.2	51.3	56.9	0.56	0.61	0.56	0.62
		10	0	172.4	135.7	143.0	135.7	135.3	0.79	0.83	0.79	0.78
		100	0	120.0	82.6	87.6	82.6	84.3	0.69	0.73	0.69	0.70
		200	0	82.9	57.5	61.3	57.5	60.3	0.69	0.74	0.69	0.73
		10	10	202.6	101.0	107.3	101.0	110.7	0.50	0.53	0.50	0.55
		100	-25	94.0	55.8	58.1	55.8	60.4	0.59	0.62	0.59	0.64
		200	50	65.3	33.3	35.8	33.3	36.8	0.51	0.55	0.51	0.56
Average				132.83	84.93	89.66	84.93	89.53	0.64	0.67	0.64	0.68

		Standard deviation		53.18	37.26	39.14	37.26	36.59	0.11	0.12	0.11	0.10
500	4	0	0	502.8	456.6	509.5	467.0	456.6	0.91	1.01	0.93	0.91
		0	10	408.2	288.1	308.3	292.2	316.0	0.71	0.76	0.72	0.77
		0	-25	298.9	185.5	193.6	187.1	274.6	0.62	0.65	0.63	0.92
		0	50	182.0	116.4	119.5	117.0	122.9	0.64	0.66	0.64	0.68
		10	0	485.3	414.0	457.0	422.5	423.7	0.85	0.94	0.87	0.87
		100	0	296.7	225.1	237.2	227.5	244.8	0.76	0.80	0.77	0.82
		200	0	198.7	149.3	154.6	150.4	162.3	0.75	0.78	0.76	0.82
		10	10	406.8	270.6	288.3	274.1	300.3	0.67	0.71	0.67	0.74
		100	-25	249.9	130.8	134.8	131.6	184.5	0.52	0.54	0.53	0.74
200	50	146.5	76.3	77.7	76.6	79.6	0.52	0.53	0.52	0.54		
Average				317.57	231.27	248.05	234.62	256.54	0.69	0.74	0.70	0.78
		Standard deviation		127.26	126.99	144.32	130.36	123.45	0.13	0.16	0.13	0.11
1500	1	0	0	47.4	39.0	39.5	39.0	39.0	0.82	0.83	0.82	0.82
		0	10	54.0	31.3	32.2	31.3	34.5	0.58	0.60	0.58	0.64
		0	-25	28.1	27.3	27.5	27.3	26.6	0.97	0.98	0.97	0.95
		0	50	28.6	17.5	18.5	17.5	22.0	0.61	0.64	0.61	0.77
		10	0	41.7	36.8	37.2	36.8	36.9	0.88	0.89	0.88	0.89
		100	0	30.5	24.3	24.3	24.3	25.1	0.80	0.80	0.80	0.82
		200	0	22.1	17.6	17.5	17.6	18.5	0.80	0.79	0.80	0.84
		10	10	52.9	29.9	30.6	29.9	33.0	0.56	0.58	0.56	0.62
		100	-25	23.2	19.1	19.1	19.1	18.4	0.82	0.82	0.82	0.79
200	50	15.4	11.3	11.6	11.3	14.3	0.74	0.76	0.74	0.93		
Average				34.39	25.41	25.79	25.41	26.83	0.76	0.77	0.76	0.81
		Standard deviation		13.65	9.03	9.14	9.03	8.63	0.13	0.13	0.13	0.11
1500	2	0	0	156.8	129.5	130.9	129.5	129.5	0.83	0.83	0.83	0.83
		0	10	163.0	97.5	100.4	97.5	112.3	0.60	0.62	0.60	0.69
		0	-25	84.0	73.9	74.4	73.9	87.5	0.88	0.89	0.88	1.04
		0	50	65.5	49.1	52.0	49.1	56.9	0.75	0.79	0.75	0.87
		10	0	132.3	121.2	122.5	121.2	122.1	0.92	0.93	0.92	0.92

		100	0	103.3	76.9	77.6	76.9	82.1	0.74	0.75	0.74	0.80
		200	0	76.5	54.7	55.1	54.7	59.8	0.72	0.72	0.72	0.78
		10	10	160.7	92.8	95.4	92.8	107.2	0.58	0.59	0.58	0.67
		100	-25	74.1	53.2	53.5	53.2	60.0	0.72	0.72	0.72	0.81
		200	50	47.4	32.4	33.6	32.4	36.8	0.68	0.71	0.68	0.78
Average				106.36	78.12	79.53	78.12	85.42	0.74	0.76	0.74	0.82
Standard deviation				43.41	31.98	32.22	31.98	31.60	0.11	0.11	0.11	0.11
1500	4	0	0	518.8	408.8	414.9	408.8	408.8	0.79	0.80	0.79	0.79
		0	10	296.6	268.3	270.9	268.3	316.0	0.90	0.91	0.90	1.07
		0	-25	242.7	177.0	178.2	177.0	272.5	0.73	0.73	0.73	1.12
		0	50	140.6	113.0	113.4	113.0	122.6	0.80	0.81	0.80	0.87
		10	0	471.1	374.3	379.5	374.3	384.4	0.79	0.81	0.79	0.82
		100	0	275.7	212.8	214.4	212.8	244.6	0.77	0.78	0.77	0.89
		200	0	184.8	143.8	144.6	143.8	159.5	0.78	0.78	0.78	0.86
		10	10	295.9	253.0	255.3	253.0	299.5	0.86	0.86	0.86	1.01
		100	-25	211.1	126.6	127.1	126.6	183.5	0.60	0.60	0.60	0.87
		200	50	109.8	74.9	75.1	74.9	79.5	0.68	0.68	0.68	0.72
Average				274.71	215.24	217.35	215.24	247.10	0.77	0.78	0.77	0.90
Standard deviation				132.26	111.34	113.36	111.34	109.78	0.09	0.09	0.09	0.13
3000	1	0	0	31.7	26.4	26.5	26.4	26.4	0.83	0.84	0.83	0.83
		0	10	35.4	22.6	22.9	22.6	26.5	0.64	0.65	0.64	0.75
		0	-25	19.6	20.4	20.5	20.4	22.1	1.04	1.05	1.04	1.13
		0	50	20.7	14.4	14.7	14.4	22.0	0.70	0.71	0.70	1.07
		10	0	27.3	25.2	25.3	25.2	25.4	0.92	0.93	0.92	0.93
		100	0	23.3	17.9	17.9	17.9	18.7	0.77	0.77	0.77	0.80
		200	0	18.3	13.6	13.5	13.6	14.1	0.74	0.74	0.74	0.77
		10	10	35.4	21.7	22.0	21.7	25.8	0.61	0.62	0.61	0.73
		100	-25	17.4	14.9	14.9	14.9	15.6	0.86	0.86	0.86	0.90
		200	50	13.6	9.5	9.6	9.5	13.8	0.70	0.70	0.70	1.02
Average				24.27	18.66	18.78	18.66	21.07	0.78	0.79	0.78	0.89

		Standard deviation	7.78	5.50	5.56	5.50	5.13	0.13	0.13	0.13	0.14	
3000	2	0	0	91.9	86.5	87.0	86.5	86.5	0.94	0.95	0.94	0.94
		0	10	90.1	70.9	71.9	70.9	86.4	0.79	0.80	0.79	0.96
		0	-25	53.1	57.6	57.8	57.6	72.2	1.08	1.09	1.08	1.36
		0	50	47.0	41.3	42.4	41.3	56.2	0.88	0.90	0.88	1.20
		10	0	76.0	82.4	82.8	82.4	83.0	1.08	1.09	1.08	1.09
		100	0	67.2	57.9	57.8	57.9	60.3	0.86	0.86	0.86	0.90
		200	0	54.8	43.5	43.3	43.5	45.1	0.79	0.79	0.79	0.82
		10	10	89.3	68.2	69.0	68.2	83.8	0.76	0.77	0.76	0.94
		100	-25	48.4	43.3	43.3	43.3	50.7	0.90	0.89	0.90	1.05
		200	50	34.8	28.1	28.4	28.1	35.1	0.81	0.82	0.81	1.01
Average			65.26	57.96	58.36	57.96	65.94	0.89	0.90	0.89	1.03	
		Standard deviation	20.63	19.08	19.21	19.08	18.95	0.12	0.12	0.12	0.16	
3000	4	0	0	474.8	247.0	247.0	247.0	247.0	0.52	0.52	0.52	0.52
		0	10	168.4	185.8	185.8	185.8	232.0	1.10	1.10	1.10	1.38
		0	-25	126.1	137.9	137.9	137.9	220.7	1.09	1.09	1.09	1.75
		0	50	92.4	93.4	93.4	93.4	107.6	1.01	1.01	1.01	1.16
		10	0	189.3	231.1	231.1	231.1	240.9	1.22	1.22	1.22	1.27
		100	0	167.3	146.2	146.2	146.2	154.9	0.87	0.87	0.87	0.93
		200	0	133.1	103.8	103.8	103.8	105.9	0.78	0.78	0.78	0.80
		10	10	167.7	176.7	176.7	176.7	216.8	1.05	1.05	1.05	1.29
		100	-25	117.0	99.6	99.6	99.6	148.4	0.85	0.85	0.85	1.27
		200	50	71.4	61.4	61.4	61.4	67.2	0.86	0.86	0.86	0.94
Average			170.74	148.27	148.27	148.27	174.15	0.94	0.94	0.94	1.13	
		Standard deviation	113.11	61.33	61.33	61.33	65.53	0.20	0.20	0.20	0.35	
Average of all 90 results			129.4	98.6	101.6	99.0	110.5	0.8	0.8	0.8	0.9	
Standard deviation of all 90 results			58.52	45.89	48.38	46.27	45.53	0.13	0.13	0.13	0.14	

Table. A3 Comparison between the results of strength for the beam-column members with C3 cross-section ($d = 300$ mm, $b_f = 50$ mm, $d_1 = 25$ mm) obtained from detailed FE models and different design methods.

Length	Thickness	Eccentricity		Capacity					Ratio of each design method prediction to the detailed FE result			
				P_{DFE} (kN)	P_{DSM} (kN)	$P_{DSM,W}$ (kN)	$P_{Distortional,W}$ (kN)	$P_{Interaction}$ (kN)	$\frac{P_{DSM}}{P_{DFE}}$	$\frac{P_{DSM,W}}{P_{DFE}}$	$\frac{P_{Distortional,W}}{P_{DFE}}$	$\frac{P_{Interaction}}{P_{DFE}}$
500	1	0	0	56.0	52.1	52.9	52.1	52.1	0.93	0.94	0.93	0.93
		0	10	60.3	41.1	43.6	41.1	45.3	0.68	0.72	0.68	0.75
		0	-25	39.2	37.6	38.0	37.6	33.7	0.96	0.97	0.96	0.86
		0	50	31.4	22.3	25.5	22.3	25.2	0.71	0.81	0.71	0.80
		10	0	52.8	47.6	48.3	47.6	48.0	0.90	0.92	0.90	0.91
		100	0	30.4	26.8	27.3	26.8	28.9	0.88	0.90	0.88	0.95
		200	0	20.3	18.1	18.4	18.1	19.9	0.89	0.91	0.89	0.98
		10	10	55.8	38.3	40.4	38.3	42.7	0.69	0.73	0.69	0.76
		100	-25	26.9	22.4	22.7	22.4	22.0	0.83	0.84	0.83	0.82
		200	50	18.8	12.4	13.4	12.4	14.2	0.66	0.71	0.66	0.75
Average				39.17	31.87	33.05	31.87	33.21	0.81	0.85	0.81	0.85
Standard deviation				15.81	13.32	13.40	13.32	13.16	0.12	0.10	0.12	0.09
500	2	0	0	199.7	172.8	174.9	172.8	172.8	0.87	0.88	0.87	0.87
		0	10	212.2	128.6	137.7	128.6	136.0	0.61	0.65	0.61	0.64
		0	-25	136.9	90.6	91.9	90.6	110.8	0.66	0.67	0.66	0.81
		0	50	120.4	63.5	74.4	63.5	66.7	0.53	0.62	0.53	0.55
		10	0	191.8	155.4	159.1	155.4	158.4	0.81	0.83	0.81	0.83
		100	0	106.9	81.5	87.6	81.5	89.0	0.76	0.82	0.76	0.83
		200	0	70.7	53.3	58.5	53.3	56.8	0.75	0.83	0.75	0.80
		10	10	197.3	118.7	127.7	118.7	128.1	0.60	0.65	0.60	0.65
		100	-25	97.2	57.1	60.4	57.1	71.3	0.59	0.62	0.59	0.73
		200	50	59.6	34.8	40.3	34.8	37.1	0.58	0.68	0.58	0.62
Average				139.27	95.63	101.24	95.63	102.69	0.68	0.72	0.68	0.73

		Standard deviation	57.08	46.38	45.96	46.38	45.60	0.11	0.10	0.11	0.11	
500	4	0	0	579.8	502.4	551.1	547.9	502.4	0.87	0.95	0.95	0.87
		0	10	481.7	353.7	377.2	375.7	360.4	0.73	0.78	0.78	0.75
		0	-25	380.8	245.0	256.0	255.3	345.5	0.64	0.67	0.67	0.91
		0	50	249.2	162.0	166.7	166.4	165.7	0.65	0.67	0.67	0.66
		10	0	568.7	444.5	483.5	479.7	456.6	0.78	0.85	0.84	0.80
		100	0	286.3	218.1	229.9	226.2	227.8	0.76	0.80	0.79	0.80
		200	0	183.7	139.3	145.2	142.5	143.9	0.76	0.79	0.78	0.78
		10	10	475.3	324.0	344.3	342.3	335.6	0.68	0.72	0.72	0.71
		100	-25	293.7	149.8	155.2	153.6	190.8	0.51	0.53	0.52	0.65
		200	50	150.1	88.0	90.3	89.3	91.6	0.59	0.60	0.59	0.61
Average			364.94	262.66	279.95	277.89	282.03	0.70	0.74	0.73	0.75	
		Standard deviation	155.42	138.85	154.23	153.58	138.34	0.10	0.12	0.12	0.10	
1500	1	0	0	54.9	46.6	46.0	46.6	46.6	0.85	0.84	0.85	0.85
		0	10	49.5	37.6	38.7	37.6	43.0	0.76	0.78	0.76	0.87
		0	-25	35.8	34.6	34.3	34.6	33.4	0.97	0.96	0.97	0.93
		0	50	25.2	21.2	23.8	21.2	25.2	0.84	0.94	0.84	1.00
		10	0	47.6	42.9	42.5	42.9	44.0	0.90	0.89	0.90	0.92
		100	0	26.9	25.3	25.2	25.3	28.6	0.94	0.94	0.94	1.06
		200	0	17.1	17.4	17.4	17.4	19.9	1.02	1.02	1.02	1.16
		10	10	45.5	35.2	36.2	35.2	40.8	0.77	0.80	0.77	0.90
		100	-25	25.2	21.3	21.2	21.3	21.9	0.85	0.84	0.85	0.87
		200	50	13.7	12.0	12.8	12.0	15.2	0.88	0.94	0.88	1.11
Average			34.13	29.40	29.81	29.40	31.86	0.88	0.89	0.88	0.97	
		Standard deviation	14.54	11.56	11.24	11.56	11.28	0.08	0.08	0.08	0.11	
1500	2	0	0	189.8	153.6	151.6	153.6	153.6	0.81	0.80	0.81	0.81
		0	10	185.8	117.6	120.8	117.6	136.0	0.63	0.65	0.63	0.73
		0	-25	116.9	85.0	84.2	85.0	109.7	0.73	0.72	0.73	0.94
		0	50	81.7	60.7	66.6	60.7	66.7	0.74	0.82	0.74	0.82
		10	0	172.7	139.7	138.8	139.7	144.9	0.81	0.80	0.81	0.84

		100	0	104.0	77.0	78.7	77.0	89.0	0.74	0.76	0.74	0.86
		200	0	67.3	51.4	53.1	51.4	56.8	0.76	0.79	0.76	0.84
		10	10	179.8	109.3	112.5	109.3	128.1	0.61	0.63	0.61	0.71
		100	-25	89.8	54.8	55.6	54.8	70.9	0.61	0.62	0.61	0.79
		200	50	51.5	34.0	36.7	34.0	37.1	0.66	0.71	0.66	0.72
Average				123.94	88.30	89.86	88.30	99.28	0.71	0.73	0.71	0.81
Standard deviation				53.25	40.18	39.06	40.18	40.77	0.08	0.08	0.08	0.07
1500	4	0	0	568.0	483.3	476.1	483.3	483.3	0.85	0.84	0.85	0.85
		0	10	399.5	344.1	340.5	344.1	360.4	0.86	0.85	0.86	0.90
		0	-25	320.7	240.3	238.5	240.3	342.3	0.75	0.74	0.75	1.07
		0	50	200.2	159.9	159.1	159.9	165.7	0.80	0.79	0.80	0.83
		10	0	513.1	429.4	424.8	429.4	450.7	0.84	0.83	0.84	0.88
		100	0	264.6	214.4	215.7	214.4	227.8	0.81	0.82	0.81	0.86
		200	0	171.2	137.7	139.5	137.7	143.9	0.80	0.81	0.80	0.84
		10	10	395.8	315.9	313.4	315.9	335.6	0.80	0.79	0.80	0.85
		100	-25	255.2	148.0	148.6	148.0	189.5	0.58	0.58	0.58	0.74
		200	50	120.5	87.4	88.1	87.4	91.5	0.73	0.73	0.73	0.76
Average				320.88	256.05	254.43	256.05	279.07	0.78	0.78	0.78	0.86
Standard deviation				146.96	132.65	129.93	132.65	134.14	0.08	0.08	0.08	0.09
3000	1	0	0	45.4	31.8	31.3	31.8	31.8	0.70	0.69	0.70	0.70
		0	10	45.7	27.3	27.6	27.3	32.1	0.60	0.60	0.60	0.70
		0	-25	28.6	25.7	25.4	25.7	30.4	0.90	0.89	0.90	1.06
		0	50	22.7	17.5	18.6	17.5	25.2	0.77	0.82	0.77	1.11
		10	0	38.9	30.0	29.6	30.0	31.6	0.77	0.76	0.77	0.81
		100	0	20.3	19.8	19.7	19.8	24.2	0.98	0.97	0.98	1.19
		200	0	11.4	14.4	14.4	14.4	17.4	1.27	1.26	1.27	1.53
		10	10	44.2	26.0	26.2	26.0	31.4	0.59	0.59	0.59	0.71
		100	-25	21.8	17.3	17.2	17.3	20.2	0.79	0.79	0.79	0.92
		200	50	12.4	10.5	11.0	10.5	13.4	0.85	0.89	0.85	1.08
Average				29.13	22.04	22.09	22.04	25.76	0.82	0.83	0.82	0.98

		Standard deviation	13.46	7.10	6.86	7.10	6.83	0.20	0.20	0.20	0.27	
3000	2	0	0	185.5	104.1	102.5	104.1	104.1	0.56	0.55	0.56	0.56
		0	10	132.8	86.2	86.1	86.2	103.6	0.65	0.65	0.65	0.78
		0	-25	85.0	67.3	66.5	67.3	101.1	0.79	0.78	0.79	1.19
		0	50	65.6	51.1	52.5	51.1	66.7	0.78	0.80	0.78	1.02
		10	0	126.8	97.5	96.5	97.5	103.3	0.77	0.76	0.77	0.81
		100	0	94.2	62.2	62.9	62.2	77.7	0.66	0.67	0.66	0.82
		200	0	65.5	44.3	45.3	44.3	55.4	0.68	0.69	0.68	0.85
		10	10	134.1	81.6	81.8	81.6	101.1	0.61	0.61	0.61	0.75
		100	-25	71.6	46.9	47.2	46.9	65.3	0.65	0.66	0.65	0.91
		200	50	40.0	30.7	31.9	30.7	37.1	0.77	0.80	0.77	0.93
Average			100.11	67.18	67.31	67.18	81.53	0.69	0.70	0.69	0.86	
		Standard deviation	43.85	24.48	23.66	24.48	24.47	0.08	0.09	0.08	0.17	
3000	4	0	0	527.1	288.6	288.6	288.6	288.6	0.55	0.55	0.55	0.55
		0	10	263.3	229.3	229.3	229.3	250.3	0.87	0.87	0.87	0.95
		0	-25	223.2	180.0	180.0	180.0	313.1	0.81	0.81	0.81	1.40
		0	50	148.1	125.8	125.8	125.8	140.4	0.85	0.85	0.85	0.95
		10	0	355.6	267.6	267.6	267.6	283.1	0.75	0.75	0.75	0.80
		100	0	237.3	161.6	161.6	161.6	183.3	0.68	0.68	0.68	0.77
		200	0	148.1	112.2	112.2	112.2	121.7	0.76	0.76	0.76	0.82
		10	10	263.4	215.8	215.8	215.8	239.0	0.82	0.82	0.82	0.91
		100	-25	184.5	120.8	120.8	120.8	167.7	0.65	0.65	0.65	0.91
		200	50	94.8	74.6	74.6	74.6	81.3	0.79	0.79	0.79	0.86
Average			244.53	177.61	177.61	177.61	206.85	0.75	0.75	0.75	0.89	
		Standard deviation	123.84	71.20	71.20	71.20	79.05	0.10	0.10	0.10	0.21	
Average of all 90 results			155.12	114.53	117.26	116.22	126.92	0.76	0.78	0.76	0.86	
Standard deviation of all 90 results			69.36	53.97	55.06	55.61	54.85	0.11	0.10	0.11	0.13	